Global Biogeochemical Cycles

RESEARCH ARTICLE
10.1029/2022GB007524

Special Section:
Understanding carbon-climate feedbacks

Resolving the Carbon-Climate Feedback Potential of Wetland CO_2 and CH_4 Fluxes in Alaska

Shuang Ma[1,2], A. Anthony Bloom[1], Jennifer D. Watts[3], Gregory R. Quetin[4], Zona Donatella[5], Eugénie S. Euskirchen[6], Alexander J. Norton[7], Yi Yin[8], Paul A. Levine[1], Renato K. Braghiere[1,8], Nicholas C. Parazoo[1], John R. Worden[1], David S. Schimel[1], and Charles E. Miller[1]

[1]Jet Propulsion Laboratory, California Institute of Technology, Pasadena, CA, USA, [2]Joint Institute for Regional Earth System Science and Engineering, University of California, Los Angeles, CA, USA, [3]Woodwell Climate Research Center, Falmouth, MA, USA, [4]Department of Geography, University of California, Santa Barbara, CA, USA, [5]Department of Biology, San Diego State University, San Diego, CA, USA, [6]Institute of Arctic Biology, University of Alaska Fairbanks, Fairbanks, AK, USA, [7]Research School of Biology, Australian National University, Canberra, ACT, Australia, [8]Division of Geological and Planetary Sciences, California Institute of Technology, Pasadena, CA, USA

Key Points:

- We use in situ measurements to constrain the modeled joint climatic sensitivity of land-atmosphere CH_4 and CO_2 exchanges
- A continued 1970-present climate trend leads to positive C-climate feedback in wet tundra sites but negative feedback in boreal and shrub fen sites
- CH_4 respiration dominates the positive tundra site feedback, CO_2 respiration dominates the negative boreal and shrub fen sites feedback

Supporting Information:

Supporting Information may be found in the online version of this article.

Correspondence to:

S. Ma,
shuang.ma@jpl.nasa.gov

Citation:

Ma, S., Bloom, A. A., Watts, J. D., Quetin, G. R., Donatella, Z., Euskirchen, E. S., et al. (2023). Resolving the carbon-climate feedback potential of wetland CO_2 and CH_4 fluxes in Alaska. *Global Biogeochemical Cycles*, *37*, e2022GB007524. https://doi.org/10.1029/2022GB007524

Received 11 JUL 2022
Accepted 24 AUG 2023
Corrected 4 OCT 2023

This article was corrected on 4 OCT 2023. See the end of the full text for details.

Abstract Boreal-Arctic regions are key stores of organic carbon (C) and play a major role in the greenhouse gas balance of high-latitude ecosystems. The carbon-climate (C-climate) feedback potential of northern high-latitude ecosystems remains poorly understood due to uncertainty in temperature and precipitation controls on carbon dioxide (CO_2) uptake and the decomposition of soil C into CO_2 and methane (CH_4) fluxes. While CH_4 fluxes account for a smaller component of the C balance, the climatic impact of CH_4 outweighs CO_2 (28–34 times larger global warming potential on a 100-year scale), highlighting the need to jointly resolve the climatic sensitivities of both CO_2 and CH_4. Here, we jointly constrain a terrestrial biosphere model with in situ CO_2 and CH_4 flux observations at seven eddy covariance sites using a data-model integration approach to resolve the integrated environmental controls on land-atmosphere CO_2 and CH_4 exchanges in Alaska. Based on the combined CO_2 and CH_4 flux responses to climate variables, we find that 1970-present climate trends will induce positive C-climate feedback at all tundra sites, and negative C-climate feedback at the boreal and shrub fen sites. The positive C-climate feedback at the tundra sites is predominantly driven by increased CH_4 emissions while the negative C-climate feedback at the boreal site is predominantly driven by increased CO_2 uptake (80% from decreased heterotrophic respiration, and 20% from increased photosynthesis). Our study demonstrates the need for joint observational constraints on CO_2 and CH_4 biogeochemical processes—and their associated climatic sensitivities—for resolving the sign and magnitude of high-latitude ecosystem C-climate feedback in the coming decades.

1. Introduction

The northern high latitudes (above 45°N) store over 50% of global soil carbon (C) (Hugelius et al., 2013; Turetsky et al., 2007). Uncertainties on the state and evolution of these C stores remain a prominent source of uncertainty in global soil C projections in terrestrial biosphere models (Wieder et al., 2019). On millennial timescales, organic C has accumulated in boreal and arctic soils as a result of slow organic C decomposition rates under cold, water-saturated, and oxygen-limited conditions (Bridgham et al., 2006). However, with temperatures across high latitude ecosystems rising faster than the global average (Box et al., 2019; Hansen et al., 2006; IPCC, 2013), present-day warming and permafrost thaw can potentially alter the balance between C gains and losses across northern high latitude ecosystems (Koven et al., 2017; Schuur et al., 2015).

Both the rate and form of C released from high latitude soils are important in understanding Earth's carbon cycle. While most soil C losses occur in the form of carbon dioxide (CO_2), when soils are water-saturated, decomposition under oxygen-deprived conditions results in the production of both CO_2 and CH_4 (Whalen, 2005). Northern high latitudes emissions alone account for 9%–27% of global wetland CH_4 emissions (Ma et al., 2022; Saunois et al., 2020). Although CH_4 emissions are typically orders of magnitude smaller than CO_2 (Bloom et al., 2016, 2017; Huntzinger et al., 2017; Melton et al., 2013), their global warming potential (GWP) is 28–34 times greater (on a 100 yr time horizon) on a mass-per-mass basis (Myhre et al., 2013). Therefore, jointly resolving CO_2 and CH_4 sensitivities to climate changes, on both C mass balance and the GWP scales, is critical for resolving northern high-latitude C-cycle feedbacks to climate change (namely the northern high latitude "carbon-climate feedbacks").

Author Contributions:

Data curation: Shuang Ma, A. Anthony Bloom, Jennifer D. Watts, Gregory R. Quetin, Zona Donatella, Eugénie S. Euskirchen

Methodology: Shuang Ma, A. Anthony Bloom, Alexander J. Norton, Yi Yin, Paul A. Levine, Renato K. Braghiere, Nicholas C. Parazoo, John R. Worden, David S. Schimel, Charles E. Miller

Validation: Shuang Ma, A. Anthony Bloom, Jennifer D. Watts, Gregory R. Quetin, Zona Donatella, Eugénie S. Euskirchen

Writing – original draft: Shuang Ma, A. Anthony Bloom

Writing – review & editing: Shuang Ma, A. Anthony Bloom, Jennifer D. Watts, Gregory R. Quetin, Zona Donatella, Eugénie S. Euskirchen, Alexander J. Norton, Yi Yin, Paul A. Levine, Renato K. Braghiere, Nicholas C. Parazoo, John R. Worden, David S. Schimel, Charles E. Miller

Spatial variability of CO_2 and CH_4 fluxes across the northern high latitudes are determined from a range of physiological and environmental gradients. Specifically, northern high latitudes CO_2 and CH_4 fluxes are regulated by a number of processes, including temperature and soil moisture controls on aerobic and anaerobic decomposition rates (Bridgham et al., 2013; Exbrayat et al., 2013; Ma et al., 2017; Riley et al., 2011), soil organic matter content and associated turnover times (Luo et al., 2017; Schädel et al., 2014; Todd-Brown et al., 2013; Wieder et al., 2019), topography and soil texture (Farquharson et al., 2019; Lipson et al., 2012; Olefeldt et al., 2016; Wang et al., 2019), landscape heterogeneity (Treat et al., 2018a, 2018b), soil pH, redox potential (Xu et al., 2016) and permafrost thaw related hydrologic responses (Lawrence et al., 2015; Rodenhizer et al., 2020).

Over the past decades, the northern high latitude ecosystems have experienced rapid shifts in climate (Box et al., 2019; Hansen et al., 2006). Due to a large number of confounding processes, substantial uncertainties preside over mechanistic representations of the temporal evolution of CO_2 and CH_4 fluxes in response to climate variability and change (Bloom et al., 2017, 2020a, 2020b; Braghiere et al., 2021; Friedlingstein et al., 2014; Melton et al., 2013; Quetin et al., 2020). On a process level, while warmer temperatures can potentially increase photosynthesis and both aerobic and anaerobic respiration rates (Huntzinger et al., 2020; Jeong et al., 2018; Piao et al., 2008; Quan et al., 2019; Reich et al., 2018; Yvon-Durocher et al., 2014), the combined effect of temperature and moisture on CO_2 and CH_4 exchanges remains unclear. Field studies find warming stimulates net CO_2 uptake under wet conditions, but has a negative effect under dry conditions (Laine et al., 2019; Quan et al., 2019; H. Zhang et al., 2020), and also indicate that the temperature response of CH_4 emission is highly dependent upon the water table status (Granberg et al., 2001; Turetsky et al., 2008; Updegraff et al., 2001; Verville et al., 1998). However, these insights alone are insufficient to mechanistically resolve how changes in climate, such as shifts in temperature and precipitation, jointly affect the bulk soil moisture, CO_2 and CH_4 respiration rates, CO_2 photosynthetic uptake, and ultimately the sign and magnitude of the total warming potential of CO_2 and CH_4 fluxes.

Jointly resolving the sign and magnitude of the CO_2 and CH_4 combined carbon-climate (C-climate) feedback is critical for quantifying the C-climate potential of wetland ecosystems in the Earth system. A modeling study shows that although the amount of CH_4 emissions was small relative to CO_2 uptake (~10% of the amount of carbon uptakes on a molar basis), the CH_4 emission (in CO_2 equivalent GWP almost entirely offset the net CO_2 uptake over the 21st century under the no-policy climate change scenario, X. Zhu et al., 2013). In response to a future warming climate, both the CH_4 source and the CO_2 sink strengthened, but the combined CH_4 and CO_2 GWP response did not show a significant trend. In a similar investigation, Lawrence et al. (2015) use the Community Land Model to show that drier soil conditions accelerate organic matter decomposition with increased CO_2 emissions, but strongly suppress growth in CH_4 emissions, and the land-to-atmosphere CO_2-equivalent C flux (namely the total CO_2 and CH_4 flux weighed by the radiative forcing of CH_4 relative to CO_2) decreases by more than 50%. While these studies provide invaluable insights on the potential role of CH_4 and CO_2 fluxes, model structures overwhelmingly rely on empirical parametrizations of CH_4 and CO_2 sensitivities to climate and soil states, which are ultimately key for accurately predicting CH_4 and CO_2 responses to a changing climate. Quantitative knowledge on the sign—and corresponding magnitude—of the C-climate feedback potential is critical for understanding the role of high latitude ecosystems in amplifying or dampening the atmospheric greenhouse gas burden in the coming decades.

Merging in situ measurements of both CO_2 and CH_4 with dynamic ecosystem models provides a unique opportunity for resolving the potential sign and magnitude of the C-climate feedbacks of wetland ecosystems. Eddy covariance (EC) flux towers provide direct and near-continuous ecosystem-scale CO_2 and CH_4 flux measurements without disturbing the soil or vegetation (Aubinet et al., 2012; Knox et al., 2019). The rapidly growing number of CO_2 and CH_4 flux tower measurements presents new opportunities for estimating fluxes at the ecosystem, regional, and global scale; furthermore, the integration of these measurements into biosphere model structures and parameters can amount to a critical step toward determining the joint sensitivities of CO_2 and CH_4 fluxes to climate variability. In turn, terrestrial biosphere models provide the necessary means to mechanistically represent the ecosystem responses to climate variability. Bayesian model-data fusion (MDF) using EC data has become a valuable tool for optimizing model C states, fluxes and process parameters and provides quantitative insights on terrestrial C cycling (Bloom & Williams, 2015; Famiglietti et al., 2020; Keenan et al., 2013; Smallman et al., 2017; Stettz et al., 2021; Williams et al., 2005; Yang et al., 2021). Model-data integration efforts also provide the C cycle mechanistic insights necessary for explicitly resolving the sensitivity of C cycling to climate and anthropogenic forcings (Bloom et al., 2020a, 2020b; Stettz et al., 2021; Yin et al., 2020).

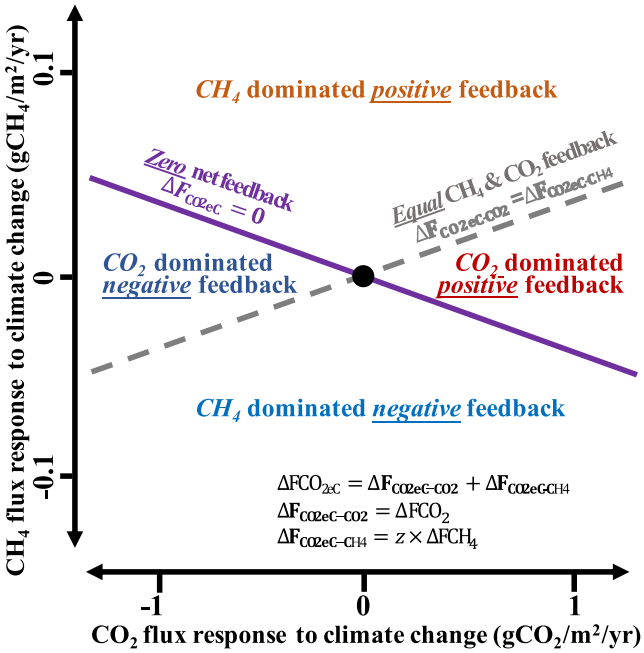

Figure 1. Conceptual diagram showing the potential responses of CH_4 (ΔCH_4 flux, *y*-axis) and CO_2 (ΔCO_2 flux, *x*-axis) to climate change, and their combined responses (ΔF_{CO_2eC}): the F_{CO_2eC} corresponds to the GWP-weighed sum of CH_4 and CO_2 flux responses to climate ($\Delta F_{CO_2eC} = \Delta F_{CO_2} + z * \Delta F_{CH_4}$), where $z = 28$ is a scalar to account for the 100-year scale GWP of CH_4 (Myhre et al., 2013). The slope of the equal feedback line is 1/28, and the slope of the zero C-climate feedback line is −1/28. The unit for both gases is gram molecular. The solid purple line denotes the "zero-feedback" line ($\Delta F_{CO_2eC-CO_2} = -\Delta F_{CO_2eC-CH_4}$), where the area above and below the solid line represents the CH_4 and CO_2 flux responses to climate as resulting in a positive (hypothesis one; H1) or negative (hypothesis two; H2) C-climate feedback. The dashed gray line represents an "equal CH_4 and CO_2 feedback line," where $\Delta F_{CO_2eC-CO_2} = \Delta F_{CO_2eC-CH_4}$, that is, CO_2 and CH_4 contribute equally to the overall F_{CO_2eC} response to climate.

In this study we investigate the potential role and magnitude of wetland CO_2 and CH_4 flux sensitivities to climate, and the sign (±) of the combined CH_4 and CO_2 climate sensitivity in terms of their combined GWP (henceforth F_{CO_2eC}, which denotes the GWP-weighed sum of CH_4 and CO_2 fluxes). To investigate the CO_2, CH_4 and F_{CO_2eC} flux responses to climate variability, we assimilate CO_2 and CH_4 EC flux tower data into a mechanistic C cycle model using the CARDAMOM Bayesian data-model integration framework (Bloom et al., 2016; Quetin et al., 2020) to constrain model parameters and states at seven EC sites in Alaska. Based on the observation-informed model analyses at each site, we probabilistically evaluate two hypotheses on the combined CO_2 and CH_4 responses to changes in climate:

H1: Climate change induces a *positive* F_{CO_2eC} response: the combined response of CO_2 and CH_4 fluxes to a change in climate—weighed by the GWP—is *greater* than 0.

H2: Climate change induces a *negative* F_{CO_2eC} response: the combined response of CO_2 and CH_4 fluxes to a change in climate—weighed by the GWP—is *less* than 0.

These hypotheses imply that wetland ecosystem responses to climate changes amount to positive (H1) or negative (H2) C-climate feedback. The two hypotheses are illustrated in Figure 1: positive land-to-atmosphere flux responses for both CH_4 and CO_2 to climate change amount to an overall positive CO_2eC response to climate (positive CC feedback), and negative land-to-atmosphere flux responses for both CH_4 and CO_2 amount to an overall negative response to climate (negative CC feedback). The combination of a negative CH_4 flux response and a positive CO_2 response, or vice versa, could amount to either a positive or negative F_{CO_2eC} response depending upon the relative contributions of CH_4 and CO_2 weighted by their GWP. Ultimately, an increase or decrease in the combined CO_2eC response of CO_2 and CH_4 to climate amounts to positive or negative C-climate feedback.

To probabilistically distinguish between the two proposed hypotheses, we quantify the EC-constrained CARDAMOM CO_2 and CH_4 flux sensitivities to individual climate variables, namely temperature and precipitation, and to hypothetical shifts in present-day climate. In Section 2, we introduce the CARDAMOM MDF approach, associated forcing data and observational constraints, and the finite difference approach for resolving CH_4 and CO_2 flux sensitivities to climate. In Section 3, we present and discuss our results, and our conclusion is in Section 4.

2. Data Description and Methods

To test the hypotheses presented in Section 1, we use the CARDAMOM MDF framework to constrain terrestrial C cycle parameters and initial model states based on in situ observations of CH_4 and CO_2 fluxes from EC towers. We introduce the structure of the process-based model used in CARDAMOM in Section 2.1; we describe the site level forcings and observational constraints in Section 2.2; we describe Bayesian MDF framework in Section 2.3; we then use the data-constrained model to determine the sensitivity of CH_4 and CO_2 fluxes to the climate in Section 2.4.

2.1. CARDAMOM Model-Data Fusion System and DALEC-JCR Model Structure

CARDAMOM is a model-data fusion (MDF) system that constrains model parameters and initial states in a process-oriented model—the Data Assimilation Linked Ecosystem Carbon model (DALEC)—and a Bayesian model-data integration algorithm using adaptive Metropolis-Hastings Markov Chain Monte Carlo (MHMCMC) (Haario et al., 2001). The DALEC model structure is uniquely suited to model-data integration, where unknown model parameters and initial states are statistically optimized to ensure minimal mismatches between ecosystem

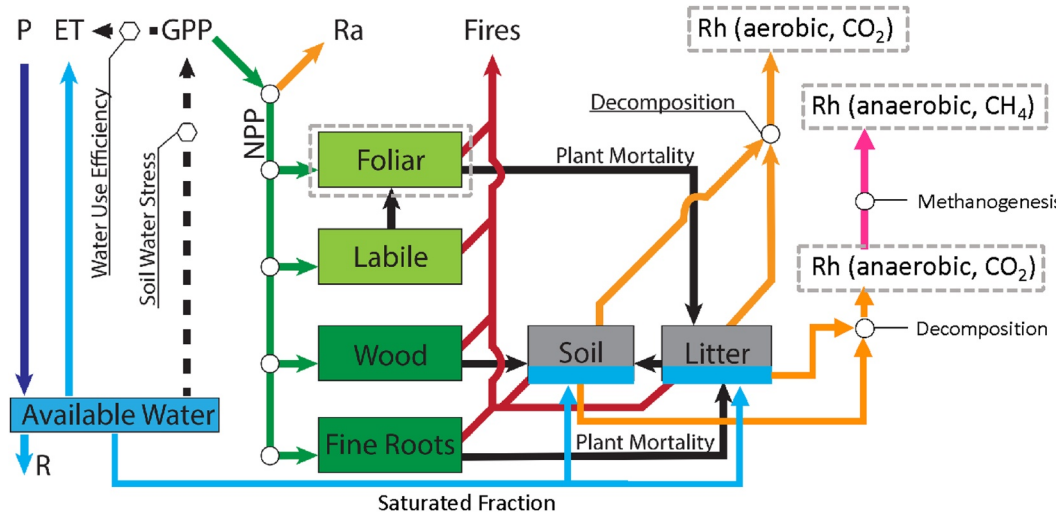

Figure 2. Diagram of DALEC-JCR, dashed gray boxes indicate modeled state variables or carbon fluxes constrained by observation data (net exchange of CO_2, and net CH_4 emission), adapted from Quetin et al. (2020), Bloom et al. (2016). *P* is precipitation, ET is evapotranspiration, *R* is runoff, GPP is gross primary production of CO_2, Ra is autotrophic respiration, and *Rh* is heterotrophic respiration. *Rh* CO_2 is simulated from anaerobic and aerobic soils, while *Rh* CH_4 emission is calculated from anaerobic soil only. The volumetric fraction of anaerobic respiration is determined by soil moisture and site-specific parameters constrained by observations. The shape of the soil moisture-respiration response curve varies across sites and is determined by site-specific observations (Figure S2 in Supporting Information S1).

observations and corresponding model states. In contrast to more complex process-based terrestrial biosphere models, the relatively parsimonious DALEC C cycle model structures employed in MDF analyses (Bloom & Williams, 2015; Famiglietti et al., 2020; Norton et al., 2023; Quetin et al., 2020; Williams et al., 2005; Yang et al., 2021) allows for joint optimization of highly uncertain process parameters (such as initial carbon and water states, photosynthetic parameters, C allocation, turnover rates and their dependencies on soil moisture) based on the available observations of carbon and water variables. While typically incorporation of complexity in models is beneficial for process representation, Famiglietti et al. (2020) show that model complexity advantages are fundamentally limited when insufficient data are available to support parameter inference.

The mechanistic knowledge gained from observations can then be used to diagnose the climatic sensitivity of land-atmosphere C fluxes and associated process controls. The DALEC model-embedded CARDAMOM MDF system has been applied to a range of spatial scales with a suite of EC and satellite data sets to (a) represent C cycles, (b) optimize critical parameters and states, and (c) infer C cycle-associated climate sensitivities (Bloom & Williams, 2015; Famiglietti et al., 2020; Norton et al., 2023; Quetin et al., 2020; Williams et al., 2005; Yang et al., 2021).

The Data-Assimilation linked Ecosystem Carbon model 2a (DALEC2a) consists of a mechanistic representation of carbon and soil water states and fluxes (Bloom et al., 2020a, 2020b; Williams et al., 2005). The six C pools—C content of foliage, labile C in plants, woody stem and coarse root, fine roots, litter, and soil organic matter—link processes such as photosynthesis, autotrophic respiration, phenology, allocation, turnover rates, fire-removed C (Bloom & Williams, 2015; Famiglietti et al., 2020; Quetin et al., 2020; Williams et al., 2005; Yang et al., 2021). The hydrological balance is defined as the sum of precipitation inputs (P) and evapotranspiration (ET) and runoff (R) outputs. In turn, the plant-available H_2O limits gross primary productivity through the conservation of the inherent water-use efficiency (Beer et al., 2009), where ET is calculated as a function of gross primary production (GPP) and atmospheric vapor pressure deficit (Bloom et al., 2020a, 2020b). Another feature of DALEC is that parameterizations per pixel/site are not based on plant functional types (PFTs). Rather, each site has its own PFT characterized by parameters that are constrained by observations. For the sake of brevity, we refer the detailed descriptions of DALEC2a by Williams et al. (2005), Bloom et al. (2020a, 2020b), Yang et al. (2021), and references therein.

Here, we extend the DALEC model structure to include a moisture and temperature-sensitive Joint CH_4 + CO_2 Respiration (JCR) scheme (Figure 2) and henceforth refer to the extended model as DALEC-JCR. We illustrate

the main features of the JCR module in the main text and explain the details in Supporting Information S1 (Text S1 and S2).

A particular challenge in Land Surface Models is the vast uncertainty in the representations of soil moisture scalar and parameterizations used to resolve respiration fluxes (Exbrayat et al., 2013). Evidence from experimental and modeling studies points to a better performance using unimodal respiration-soil moisture response curve, rather than a linear relationship (Cox, 2001; Exbrayat et al., 2013; Sitch et al., 2003). A less well-characterized mechanism in models is how soil properties and vegetation types change the shape of optimum soil moisture response curves, which is found to be important for predicting the response of soil carbon to future climate scenarios (Moyano et al., 2012).

To address this challenge within a MDF framework, DALEC-JCR resolves site-specific data-constrained parameters to characterize the shape of the soil moisture-respiration curve (Text S2 in Supporting Information S1). While CH_4 production occurs as long as anaerobic conditions occur at a microscopic scale, water is not evenly distributed within the spatial domain of the target site, not least due to topographic heterogeneity, along with variability in other edaphic and biotic factors. Therefore, we expect anaerobic respiration to increase gradually—rather than step-wise—with increasing soil moisture. To account for this in DALEC-JCR, we diagnostically determine the dynamics of the aerobic fraction of the soil column based on an empirical continuous functional relationship between soil moisture and aerobic soil fraction (Text S1 in Supporting Information S1).

In the DALEC JCR module, CO_2 is respired both anaerobically and aerobically—from oxic and anoxic soil conditions, respectively—while CH_4 is only respired anaerobically. The JCR module calculates aerobic and anaerobic respiration from the soil column separately, both as a function of C turnover rate, soil temperature, soil moisture, and volumetric fraction of aerobic/anaerobic soil:

$$Rh_{\mathrm{ae}} = C_{\mathrm{litter}} k_{\mathrm{litter}} f_{V_{\mathrm{ae}}} f_W f_T f_{\mathrm{lit2som}} + C_{\mathrm{SOM}} k_{\mathrm{SOM}} f_{V_{\mathrm{ae}}} f_W f_T, \quad (1)$$

$$Rh_{\mathrm{an}} = C_{\mathrm{litter}} k_{\mathrm{litter}} \left(1 - f_{V_{\mathrm{ae}}}\right) f_{Wc} f_T f_{\mathrm{lit2som}} + C_{\mathrm{SOM}} k_{\mathrm{SOM}} \left(1 - f_{V_{\mathrm{ae}}}\right) f_{Wc} f_T, \quad (2)$$

where C_{litter} and C_{SOM} are the litter and soil organic matter C pool size; k_{litter} and k_{SOM} are the basal decay rate of C pools, their value are independent of respiration type; f_W is the soil moisture scalar on aerobic respiration rate; f_{Wc} is the soil moisture scalar when the soil is saturated; the anaerobic soil is saturated (soil moisture always equals one) and thus the soil moisture scalar is given a constant value of f_{Wc} in Equation 2, the value of f_{Wc} is determined at each individual site and constrained by observations in our data-model fusion framework; $f_{V_{\mathrm{ae}}}$ is the aerobic fraction of the vertical soil column; $1 - f_{V_{\mathrm{ae}}}$ is the anaerobic fraction of the soil. Equations S1–S4 in Supporting Information S1 describe how f_W and $f_{V_{\mathrm{ae}}}$ are calculated; f_T is the soil temperature scalar on respiration rate:

$$f_T = Q_{10}^{\frac{T - T_{\mathrm{mean}}}{10}}, \quad (3)$$

where Q_{10} is the factor by which respiration rate increases with a 10°C increase in temperature. T is the mean air temperature of the current time step, T_{mean} is the multi-year mean air temperature at the region.

The heterotrophic respiration terms in the form of CO_2 (Rh_{CO_2}) and CH_4 (Rh_{CH_4}) are then calculated as:

$$Rh_{\mathrm{CO_2}} = Rh_{\mathrm{ae}} * 1 + Rh_{\mathrm{an}} * \left(1 - f_{\mathrm{CH_4}}\right), \quad (4)$$

$$Rh_{\mathrm{CH_4}} = Rh_{\mathrm{ae}} * 0 + Rh_{\mathrm{an}} * f_{\mathrm{CH_4}}, \quad (5)$$

where f_{CH_4} is the fraction of CH_4 in anaerobic respiration:

$$f_{\mathrm{CH_4}} = r_{\mathrm{CH_4}} * Q_{10_{\mathrm{CH_4}}}^{\frac{T - T_{\mathrm{mean}}}{10}}, \quad (6)$$

where r_{CH_4} is the potential ratio of anaerobically mineralized C released as CH_4; $Q_{10_{CH_4}}$ is the factor by which CH_4 production rate increases with a 10°C increase in temperature, on top of the temperature sensitivity encountered in Equations 1 and 2 (f_T); The reason we put a $Q_{10_{CH_4}}$ on top of the general respiration temperature sensitivity term here is that studies have found higher temperature sensitivity in methane production than CO_2 respiration across microbial to ecosystem scales (Yvon-Durocher et al., 2014). T is the mean air temperature of the current time step, T_{mean} is the multi-years mean air temperature at the region.

Table 1
Mean and Inter-Annual Variation (IAV) During 2001–2016, and the Trend of Temperature and Precipitation During 1970–2016 at the Eddy Covariance Sites

AmeriFlux site ID (references)	Latitude/Longitude/Wetland characteristics	Vegetation type	ERA-interim temperature			ERA-interim precipitation		
			MAT (2001–2016, °C)	IAV (2001–2016, °C)	Trend (1970–2016, °C/yr)[a]	MAP (2001–2016, mm)	IAV (2001–2016, mm)	Trend (1970–2016, mm/yr)[a]
US-ICs (Euskirchen et al., 2017)	68.6/−149.3/wet tundra fen (alkaline)	Wet sedge and dwarf shrubs	−9.4	0.83	0.039	426	75	1.47
US-BZB (Euskirchen et al., 2014)	64.7/−148.3/thermalkarst bog (acidic)	Lowland boreal forests	−1.5	0.94	0.039	413	49	1.55
US-Bes (Davidson et al., 2016)	71.3/−156.6/wet tundra (acidic)	Sedges, grasses, moss, lichens	−9.5	0.96	0.038	244	34	1.47
US-Beo (Davidson et al., 2016)	71.3/−156.6/wet tundra (acidic)	Sedges, grasses, moss, lichens	−9.5	0.96	0.038	244	34	1.47
US-Brw (Davidson et al., 2016)	71.3/−156.6/wet tundra (acidic)	Sedges, grasses, moss, lichens	−9.5	0.96	0.038	244	34	1.47
US-Atq (Davidson et al., 2016)	70.5/−157.4/wet tundra (acidic)	Moist sedge, tussock	−9.6	1.00	0.038	263	42	1.54
US-Ivo (Davidson et al., 2016)	68.49/−155.8/wet tundra (acidic)	Tussock sedge, moss	−9.4	0.93	0.038	462	53	1.40

Note. Mean and IAV during 2001–2016 are directly calculated from ERA-interim data.
[a]ERA-interim trend during 1970–2016 is converted from NCEP data: $ERA\_trend_{(1970–2016)} = NCEP\_trend_{(1970–2016)} * ERA\_IAV_{(2001–2016)}/NCEP\_IAV_{(1970–2016)}$.

The parsimonious DALEC-JCR model structure (Figure 2) does not represent a range of soil hydrological and physical states, such as soil energy dynamics, permafrost thaw, snow cover, snowmelt infiltration, and soil consumption of CH_4. To determine if the DALEC-JCR model, with data-informed parameters, can simulate realistic observable CO_2 and CH_4 fluxes (i.e., NEE and CH_4), we compare their temporal variability to fluxes from a more structurally complex and comprehensive ecosystem model (Terrestrial ECOsystem 2.0, TECO 2.0, Weng & Luo, 2008), at a well-calibrated bog site in northern Minnesota (Ma et al., 2017). TECO 2.0 is a process-based ecosystem model that has six submodules: canopy, vegetation dynamics, soil water, soil energy (including snow cover, thermal dynamics, and frozen depth), soil carbon/nitrogen, and aerobic/anaerobic respirations (CO_2 and CH_4). TECO 2.0 explicitly represents the transient and vertical dynamics of soil moisture, soil temperature, liquid fraction, frozen depth, CH_4 production, oxidation, and major transport pathways (diffusion, ebullition, and plant-mediated-transport); a bucket model is used to estimate water table level, determined by soil moisture change. The aerobic and anaerobic zones are separated at the water table (Granberg et al., 1999; Wania et al., 2010; Q. Zhu et al., 2014). A detailed description of TECO is available in Weng and Luo (2008) and Ma et al. (2017, 2023). The DALEC-JCR emulation of TECO 2.0 is described in the manuscript supplement (Text S3 in Supporting Information S1); We find DALEC-JCR performs favorably against the TECO 2.0 variability in CO_2 and CH_4 fluxes ($R^2_{CO_2} = 0.92$; $R^2_{CH_4} = 0.8$, Figure S12 in Supporting Information S1), which corroborates the overall DALEC-JCR model structure.

2.2. Model Forcings and Observation Constraints

We configure DALEC-JCR forcings and observation constraints at seven high-latitude eddy tower sites (Table 1 and Figure S3 in Supporting Information S1). Five sites are low-lying vegetation wet tundra (sedge grasses, moss, lichen, US-Bes, US-Beo, US-Brw, US-Atq, US-Ivo), one site is fen covered by shrubs, grasses, and moss (US-ICs), and one site is boreal bog covered by trees, shrubs, grasses, and moss (US-BZB). Following Bloom and Williams (2015), we provide a continuous monthly meteorological forcing data set for DALEC-JCR using 0.5° resolution meteorological forcing (namely monthly temperature, precipitation, global incident shortwave radiation, vapor pressure deficit, and burned area) obtained from the European Centre for Medium-Range Weather Forecasts (ECMWF) Reanalysis Interim (ERA-interim, Berrisford et al., 2011) to drive DALEC-JCR model at each site. The model was run at a monthly timestep. Basic information about the EC sites is listed in Table 1. We use monthly averaged net CH_4 and CO_2 fluxes to constrain DALEC-JCR (see Section 2.3); months with less than 10 days of observations are excluded from our analysis.

2.3. Bayesian Model-Data Fusion Framework

We optimize JCR module parameters (Table S1 in Supporting Information S1)—along with other DALEC time-invariant model parameters and initial C and H_2O states (in total 33 time-invariant parameters and 8 initial states)—within the CARDAMOM (CARbon Data Model fraMework) MDF system. The CARDAMOM model parameters are independently optimized at each one of the seven flux tower sites. The CARDAMOM framework uses Bayes' theorem to optimize the posterior probability of initial states and time-invariant process parameters ($\boldsymbol{y}$), given observations $\boldsymbol{O}$, $p(\boldsymbol{y}|\boldsymbol{O})$, as follows:

$$p(\boldsymbol{y}|\boldsymbol{O}) \propto p(\boldsymbol{y})p(\boldsymbol{O}|\boldsymbol{y}) \quad (7)$$

where $p(\boldsymbol{y})$ is the prior probability distribution of $\boldsymbol{y}$, and $p(\boldsymbol{O}|\boldsymbol{y})$ is proportional to the likelihood of $\boldsymbol{y}$ given $\boldsymbol{O}$, $L(\boldsymbol{y}|\boldsymbol{O})$. At each tower site, the observation vector $\boldsymbol{O}$ consists

Table 2
Climate Perturbation Scenarios

Climate scenarios	Short name	Purpose	Description	Climate perturbation
S1	Warmer	Reflect year-to-year changes, based on the historical Inter Annual Variation (IAV) of 2001–2016	A hypothetical increase/decrease in temperatures relative to nominal IAV	Standard deviation of mean annual temperature (MAT) ($+\boldsymbol{\sigma}_{temp}$, unit °C/yr)
S2	Wetter		A hypothetical increase/decrease in precipitation relative to nominal IAV	Standard deviation of mean annual precipitation (MAP) ($+\boldsymbol{\sigma}_{prec}$, unit mm/yr)
S3	Warmer + Wetter		A hypothetical increase in temperatures and precipitation relative to nominal IAV. To test sensitivity of CO_2 and CH_4 to warming and wetting	Standard deviation of MAT and MAP ($\boldsymbol{\sigma}_{temp} + \boldsymbol{\sigma}_{prec}$)
S4	Warmer + Drier		A hypothetical increase in temperatures and decrease in precipitation relative to nominal IAV. To test sensitivity of CO_2 and CH_4 to warming and drying	Standard deviation of MAT and MAP ($\boldsymbol{\sigma}_{temp} - \boldsymbol{\sigma}_{prec}$)
S5[a]	1971–2016 trend (warmer and wetter at all sites)	General trend	A hypothetical increase in temperatures and precipitation following the 50 years trend. To test sensitivity of CO_2 and CH_4 to continuation of 50 years climate change trend	50 years trend, slope of linear regression ($\boldsymbol{\tau}_{temp} + \boldsymbol{\tau}_{prec}$) (units $\boldsymbol{\tau}_{temp}$ °C/yr; $\boldsymbol{\tau}_{prec}$ mm/yr)

[a]Sensitivities of CO_2 and CH_4 to continuation of 50 years climate change trend in the growing (June-August) and nongrowing (September-May) seasons are also tested; results are shown in Figure S15 in Supporting Information S1.

of measurements including the NEE, and CH_4. Assuming errors are uncorrelated, the overall likelihood of $\boldsymbol{y}$ given $\boldsymbol{O}$ can be expressed as

$$L(y|O) = L_{NEE}\, L_{CH_4} \tag{8}$$

For NEE and CH_4 we derive the corresponding likelihood function L_* (i.e., L_{NEE}, and L_{CH_4}) as follows:

$$L_* = e^{-\frac{1}{2}} \sum_i \left(\frac{m_i(y) - o_i}{\sigma_i} \right)^2 \tag{9}$$

where o_i and $m_i(\mathbf{y})$ correspond to the ith observation and the corresponding modeled quantity derived from control vector $\mathbf{y}$, respectively; σ_i accounts for the combined errors from the DALEC model structure, forcing drivers, and observations. Following (Bloom et al., 2020a, 2020b), we retrieve the distribution of p($\mathbf{y}$|O) at each tower site by running four adaptive MHMCMC chains for 10^8 iterations. We used the Gelman–Rubin statistic (Gelman & Rubin, 1992) to check the convergence of sampling chains. The first half of the accepted parameters was discarded as the burn-in period, and the second half was used for posterior analysis. We evaluate modeled CO_2 and CH_4 fluxes against observed ones using the RMSE normalize by the standard deviation (NRMSE), and coefficient of determination (R_2).

2.4. Climate Perturbations

To characterize the potential role of climate variability on CH_4 and CO_2 fluxes, we focus on warming and precipitation from a regional perspective to diagnostically resolve CO_2/CH_4 sensitivities and the sign of their combined feedback (Figure 1, H1-H2). To estimate the net F_{CO_2eC} response (the GWP-weighed sum of CO_2 and CH_4 fluxes) to climate change, we designed five likely climate change scenarios based on the 2001–2016 Inter-annual Variation (IAV) (scenarios S1–S4, ERA Interim) and 1970–2016 temperature and precipitation trends (scenario S5, CRU-NCEP reanalysis) (Figure S4 in Supporting Information S1, Table 2). ERA Interim is used due to its consistency with model driver data, and is broadly consistent with gap-filled FLUXNET CH_4 meteorology data (Vuichard & Papale, 2015). We use the CRU-NCEP reanalysis data to quantify the scenario S5 climate variable trends, the CRU-NCEP data set covers a substantially longer time period (1901–2016). The CRU-NCEP centennial temperature variability (shown in Figure S4 in Supporting Information S1) reveals a steep increase of temperature beginning in 1970 (in contrast to the 1901–1970 time period); we therefore chose to use 1970–2016 trend to characterize scenario S5 climate trends (Table 2).

To quantitatively resolve H1 and H2, we denote the modeled C fluxes, $\boldsymbol{F}$, as a function of time-dependent meteorological drivers ($\boldsymbol{M}$) and time-invariant model parameters and initial states ($\boldsymbol{y}$):

$$\boldsymbol{F} = \text{DALEC} - \text{JCR}(\boldsymbol{M}, \boldsymbol{y}) \tag{10}$$

where the DALEC-JCR() operator denotes the DALEC-JCR model simulation driven by forcing $\boldsymbol{M}$ and parameters $\boldsymbol{y}$.

We take two steps to evaluate the responses of CO_2 and CH_4 fluxes to decadal-scale climate change:

2.4.1. STEP 1: Deriving Flux Sensitivity to Climate Changes

We calculate the local gradient of $\boldsymbol{F}$ response curve against environment variables ($\boldsymbol{M}$) by perturbing $\boldsymbol{M}$ with an arbitrarily small change to $\boldsymbol{M}$, Δm (e.g., $\Delta m = 1e^{-5}$°C for temperature dimension, $\Delta m = 1e^{-8}$ mm/day for precipitation dimension), where:

$$\boldsymbol{dF/dM} \approx \Delta \boldsymbol{F}/\Delta m = (\mathrm{DALEC}(\boldsymbol{M} + \Delta m_{\to 0}, \boldsymbol{y}) - \mathrm{DALEC}(\boldsymbol{M}, \boldsymbol{y})/(\Delta m_{\to 0})) \tag{11}$$

To calculate the uncertainty of $\boldsymbol{dF/dM}$, we use 4,000 samples of $\boldsymbol{y}$ accepted from the CARDAMOM Bayesian inversion (Section 2.3) and for each one we derive the corresponding dF/dM values from Equation 11. We derive $\boldsymbol{dF/dM_T}$ (temperature) and $\boldsymbol{dF/dM_P}$ (precipitation) using Equation 11. The combined effects of temperature and precipitation, $\boldsymbol{dF/dM_{TP}}$ can be expressed as:

$$\frac{\boldsymbol{dF}}{\boldsymbol{dM_{TP}}} = \frac{\boldsymbol{dF}}{\boldsymbol{dM_T}} + \frac{\boldsymbol{dF}}{\boldsymbol{dM_P}} + \boldsymbol{I} \tag{12}$$

where $\boldsymbol{I}$ represents the interactions between **P** and **T** anomalies on C fluxes. We tested the interactions between temperature and precipitation effects (shown in supplementary Text S4 in Supporting Information S1) and found it is more than an order of magnitude smaller than the individual effects; we therefore approximate combined temperature and precipitation effects as

$$\frac{\boldsymbol{dF}}{\boldsymbol{dM_{TP}}} \sim \frac{\boldsymbol{dF}}{\boldsymbol{dM_T}} + \frac{\boldsymbol{dF}}{\boldsymbol{dM_P}} \tag{13}$$

2.4.2. STEP 2: C Flux Responses to Change in Climate

We estimate the C flux response ($\Delta \boldsymbol{F}$) to a change in climate using the following equation:

$$\Delta \boldsymbol{F} = \frac{\boldsymbol{dF}}{\boldsymbol{dM}} \Delta \boldsymbol{M} \tag{14}$$

where $\Delta \boldsymbol{M}$ represents a climate anomaly (Table 2, either the 2001–2016 inter-annual variability (IAV) or the 1970-present trends of temperature and precipitation). The flux sensitivity to climate derived here represent the contemporary integrated sensitivity to climate variability, with the assumption that the integrated responses of C fluxes $\Delta \boldsymbol{F}$ to climate changes Δm can be linearly approximated as $\Delta \boldsymbol{F} = \Delta m \boldsymbol{dF/dM}$. We discuss this assumption and its limitations in Section 3.3.

Using Equation 14, we calculate individual C flux responses to individual climate variables. We then estimate the joint F_{CO_2eC} effect of CO_2 and CH_4 to temperature changes, $\Delta \boldsymbol{T}$, as follows:

$$\Delta \boldsymbol{F}_{\mathrm{CO_2eC}(T)} = \frac{\boldsymbol{dF}_{\mathrm{CO_2eC}}}{\boldsymbol{dM_T}} \Delta \boldsymbol{T} = \left(\frac{\boldsymbol{dF}_{\mathrm{CO_2}}}{\boldsymbol{dM_T}} + \boldsymbol{z} \frac{\boldsymbol{dF}_{\mathrm{CH_4}}}{\boldsymbol{dM_T}} \right) \Delta \boldsymbol{T} \tag{15}$$

where $\Delta \boldsymbol{F}_{\mathrm{CO_2eC}(T)}$ denotes the CO_2 equivalent C flux response, and z is the GWP of CH_4

Similarly, we derive the joint F_{CO_2eC} CO_2 and CH_4 response to precipitation changes as follows:

$$\Delta \boldsymbol{F}_{\mathrm{CO_2eC}(P)} = \frac{\boldsymbol{dF}_{\mathrm{CO_2eC}}}{\boldsymbol{dM_P}} \Delta \boldsymbol{P} = \left(\frac{\boldsymbol{dF}_{\mathrm{CO_2}}}{\boldsymbol{dM_P}} + \boldsymbol{z} \frac{\boldsymbol{dF}_{\mathrm{CH_4}}}{\boldsymbol{dM_P}} \right) \Delta \boldsymbol{P} \tag{16}$$

For Scenarios 1–4 (S1–S4), we derive ΔP and ΔT as a 1σ perturbation to mean 2001–2016 precipitation, where 1-σ represents the 2001–2016 IAV of annually averaged P and T, respectively. For Scenario 5 ΔP and ΔT are the 1970-present trend (τ) of temperature and precipitation. The joint effects of CO_2 and CH_4 in a warmer and wetter scenario is then equal to:

$$\Delta \boldsymbol{F}_{\mathrm{CO_2eC}} = \Delta \boldsymbol{F}_{\mathrm{CO_2eC}(T)} + \Delta \boldsymbol{F}_{\mathrm{CO_2eC}(P)} \tag{17}$$

and a warmer and drier scenario is

$$\Delta \boldsymbol{F}_{\mathrm{CO_2eC}} = \Delta \boldsymbol{F}_{\mathrm{CO_2eC}(T)} - \Delta \boldsymbol{F}_{\mathrm{CO_2eC}(P)} \tag{18}$$

In subsequent sections, we denote the CH_4 and CO_2 components of $\boldsymbol{F}_{CO_2eC}$ as $\boldsymbol{F}_{CO_2eC-CH_4}$ and $\boldsymbol{F}_{CO_2eC-CO_2}$ respectively, where

$$\boldsymbol{F}_{CO_2eC} = \boldsymbol{F}_{CO_2eC-CO_2} + \boldsymbol{F}_{CO_2eC-CH_4}, \quad (19)$$

and use $\boldsymbol{\Delta F}_{CO_2eC-CH_4}$ and $\boldsymbol{\Delta F}_{CO_2eC-CO_2}$ to denote associated changes. The sign and magnitude of CO_2eC response to climate ($\boldsymbol{\Delta F}_{CO_2eC}$) can be used to quantitatively evaluate the C-climate feedback potential of wetland ecosystems.

3. Results and Discussion

3.1. Evaluation of Model Performance and Parameters

The seasonal variability and IAV of EC net CO_2 and CH_4 at all sites are captured by DALEC-JCR: the normalized RMSE (NRMSE) ranges are 0.15–0.0.37 (CO_2) and 0.33–0.9 (CH_4), R^2 ranges 0.90–0.97 (CO_2) and 0.30–0.90 (CH_4) (Figure 3, Figures S5–S11 in Supporting Information S1). R^2 of modeled CO_2 and CH_4 fluxes are higher at sites with over 1 year of observations. The model captures cold season (September to May) CH_4 emissions, which is found to dominate the Arctic tundra CH_4 budget but is not currently well simulated in most terrestrial biosphere models (Zona et al., 2016). Modeled cold season CH_4 emissions account for 32%–66% of the annual budget across seven Alaskan sites, comparable to the estimations based on in situ observations from the same time periods (37%–64%, US-Bes, US-Beo, US-Brw, US-Atq, and US-Ivo, Zona et al., 2016): Notably, the model captures the sudden decrease of CH_4 at the end of the growing season and autumn (August and September) due to a decrease in soil moisture and thus lower anaerobic soil fraction at US-Beo, US-Bes, US-Brw (Figures S7–S9 in Supporting Information S1). In situ observations at those sites indicate lowest water table depth in the same period (Zona et al., 2016). Both the model and in situ measurements show a 1-month-delayed drop in soil moisture (August) in response to decreased precipitation (June-July), which could be due to the replenishment from thawing permafrost (Figures S7–S9 in Supporting Information S1).

The temperature sensitivity of heterotrophic CO_2 respiration (Q_{10}Rh) ranges from 1.3 to 1.8 (mean of posterior distribution from the seven sites), and $Q_{10}CH_4$ ranges from 1.1 to 2.2, and the range of CH_4/CO_2 potential (rCH_4) is 0.1–0.3. These posterior parameter estimates generally fall within the empirical ranges we found in the literature (Riley et al., 2011) and are consistent across sites in similar latitudes and vegetation communities (Figure S13 in Supporting Information S1).

The regression between aerobic respiration and soil moisture follows a unimodal curve (the C2 response curve in Figure S2 in Supporting Information S1) at US-ICs, and a logarithmic curve (Figure S2 C1 in Supporting Information S1) at all the other sites. As shown in Figure S2 in Supporting Information S1, a unimodal response curve indicates that soil saturation suppresses aerobic CO_2 respiration, a logarithmic curve indicates no suppression on aerobic CO_2 respiration in saturated soils. At US-ICs, we find that aerobic CO_2 respiration peaks when soil moisture is at 70%, and saturated soils suppress the heterotrophic respiration rates by 60%. Notably, US-ICs is a fen ecosystem, characterized as a peat-forming wetland relying on groundwater input, with low to moderate soil alkalinity (pH = 5.5–6.9), while all the other sites (bog and wet tundra) have acidic soil (pH = 3.3–5.5) (Bourbonniere, 2009; Clymo et al., 1984). Our finding potentially indicates that redox potential (as a result of different pH) is a key determinant of how soil moisture controls aerobic respiration, as found in numerous studies (Bhanja & Wang, 2020; Brewer et al., 2018; Fiedler et al., 2007; Porter et al., 2004).

3.2. Combined Climatic Responses of CH_4 and CO_2 Fluxes

We find that warming and wetting alone increase CH_4 emissions across all sites. Temperature induces a +0.07 to +0.36 $gCH_4/m^2/yr/\sigma_T$ and precipitation induces a +0.45 to +1.69 g $CH_4/m^2/yr/\sigma_P$ response across all sites, where σ_T and σ_P represent a 1σ climate perturbation in temperature and precipitation, respectively (the ranges encompass median values from the seven sites). Warming accelerates net CO_2 loss at all sites (+1.7 to +27.6 $gCO_2/m^2/yr/\sigma_T$), while precipitation can change net CO_2 in both directions (−203.2 to +18.3 $gCO_2/m^2/yr/\sigma_P$). We find warming alone increased F_{CO_2eC} at all seven high-latitude sites: CH_4 component of F_{CO_2eC} ($F_{CO_2eC-CH_4}$) plays a larger role than the CO_2 component of F_{CO_2eC} ($F_{CO_2eC-CO_2}$) at two of the sites (US-BZB, a boreal wetland site near Fairbanks, Alaska, and US-BES, a tundra site near Utqiagvik), and CH_4 component of F_{CO_2eC} players a smaller role than the CO_2 component at the other sites (Figure 4a, Figure S14a in Supporting Information S1). We find

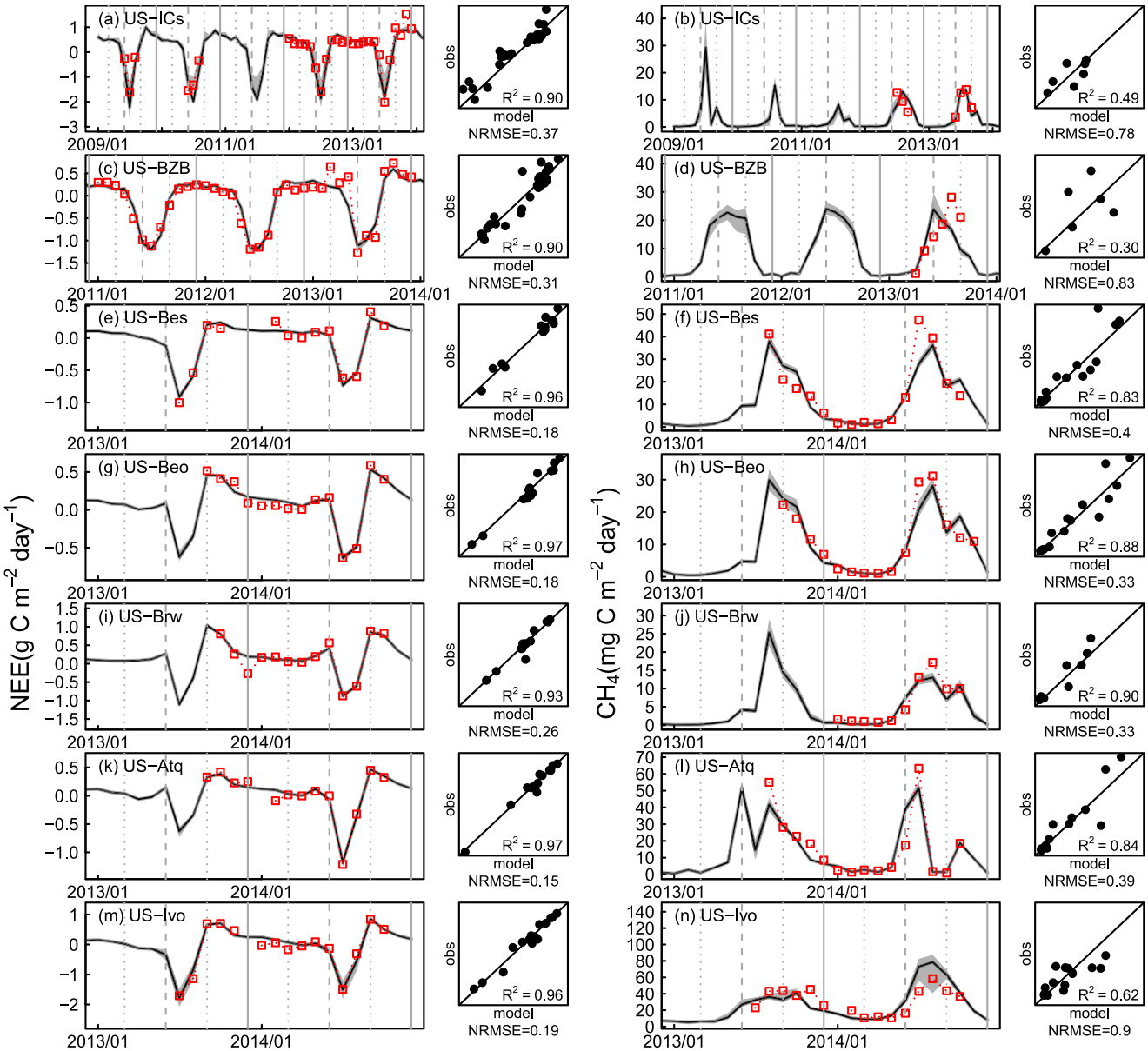

Figure 3. DALEC-JCR modeled CO_2 and CH_4 at seven Alaska sites, jointly constrained by Eddy covariance (EC) CH_4 and CO_2 flux measurements. Red squares are monthly aggregated eddy flux observations. Black lines are the modeled median of 4,000 random samples from posterior estimates constrained by EC NEE and CH_4 data, gray shades are the 5–95 percentile interval. Vertical gray lines represent March (dotted), June (dashed), September (dotted), and December (solid). Location of these sites on a map is shown in Figure S3 in Supporting Information S1.

that the impacts of a 1σ change in precipitation are on average five-fold larger than 1σ change in temperature for CH_4 (Figures 4a and 4b).

In terms of the combined CH_4 + CO_2 responses (F_{CO_2e-C}), a 1σ change in precipitation induces a larger response than a 1σ change in temperature (CO_2 equivalent responses are −168.3 to +65.6 gCO_2 eC/m^2/yr/σ_T and +8.3 to +31.4 gCO_2 eC/m^2/yr/σ_P, respectively) at all sites. Although net CH_4 fluxes are at least 10 times smaller than CO_2, the impact of a 1σ increase in temperature and precipitation (Scenario 3) on $\Delta F_{CO_2eC-CH_4}$ is larger than $\Delta F_{CO_2eC-CO_2}$ at four sites ($\Delta F_{CO_2eC-CH_4}/\Delta F_{CO_2eC-CO_2}$ = 1.2–2.8 fold, range of medians). However, at US-BZB, US-ICs, and US-Brw, we find $\Delta F_{CO_2eC-CH_4} < \Delta F_{CO_2eC-CO_2}$ ($\Delta F_{CO_2eC-CH4}/\Delta F_{CO_2eC-CO_2}$ = 0.22–0.38 fold, range of medians) (Figure 5a).

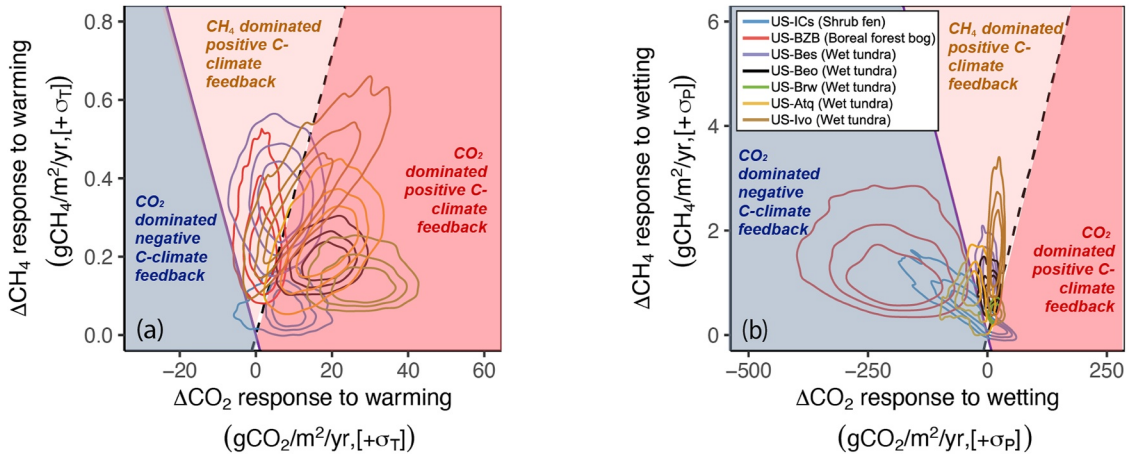

Figure 4. Responses of net CO_2 and CH_4 fluxes to 1σ changes in temperature or precipitation: (a) Scenario 1, warmer ($+\sigma_{temp}$); and (b) Scenario 2, wetter ($+\sigma_{prec}$). See Table 2 for reference to Scenario 1 and Scenario 2. Each color represents one single site and the contour lines are two-dimensional kernel density derived from 4,000 random samples from posterior estimate constrained by eddy covariance net CO_2 and CH_4 data (50%, 75%, and 95% distributions) derived from CARDAMOM posterior states and parameters. Refer to Figure 1 for descriptions of lines and intersections.

3.3. Biogeochemical Controls on CO_2 and CH_4 Flux Climate Sensitivities

We found that a warmer and wetter climate induces a positive F_{CO_2eC} response (ΔF_{CO_2eC} = 17.7–88.2 gCO_2 eC/m2/yr) in wet tundra sites but a negative F_{CO_2eC} in the fen and bog sites (ΔF_{CO_2eC} = 15.8–159.7 gCO_2 eC/m^2/yr), where heterotrophic respiration dramatically decreases due to increased soil moisture and is accompanied by increased photosynthesis (Figure S14 in Supporting Information S1). The bog site (US-BZB) is the only site with boreal forest, thus the ecosystem has a larger leaf biomass and litter pool to facilitate a quick response of C decomposition and uptake. The fen site (US-ICs) is also unique from the other wet tundra sites due to the presence of shrub species (larger plant biomass) and alkaline soil (resulting a different redox potential), which may drive a stronger response in both heterotrophic respiration and photosynthesis. de Vrese et al. (2021) predicted weak soil CO_2 respiration in the wet months of the year, which led to low soil CH_4 fluxes in permafrost regions under Shared Socioeconomic Pathway 5 and the Representative Concentration Pathway 8.5. We predict the same directional changes in soil CO_2 respiration due to increased soil moisture, but increased CH_4 due to warmer temperature and larger anaerobic fraction in the soil column. Shu et al. (2020) predict CH_4 increase by 30% and 64% at the

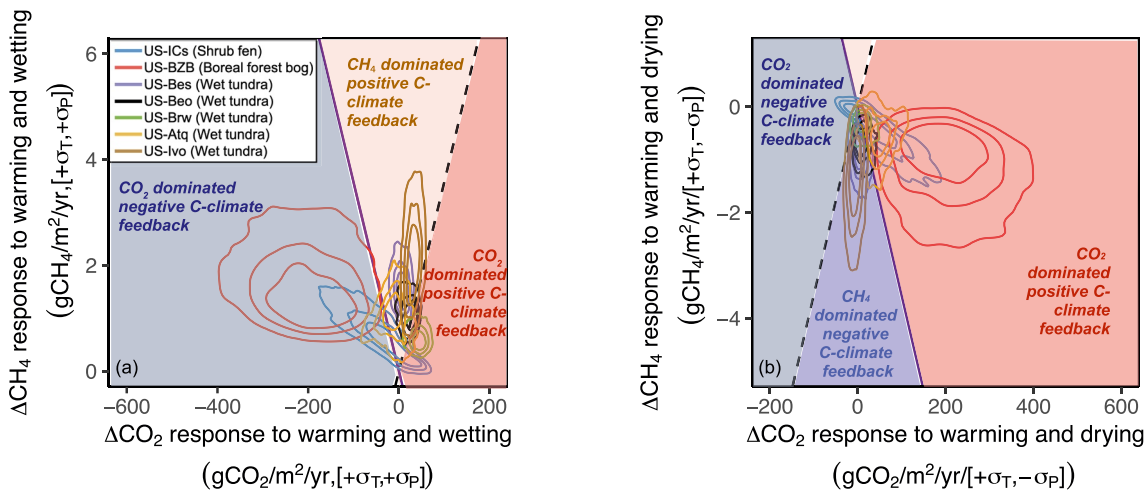

Figure 5. Responses of wetland CO_2 and CH_4 fluxes to 1σ changes in temperature and precipitation at high-latitude sites: (a) Scenario 3, warmer and wetter ($+\sigma_{temp}$, $+\sigma_{prec}$); and (b) Scenario 4, warmer and drier ($+\sigma_{temp}$, $-\sigma_{prec}$). See Table 2 for reference to Scenario 3 and Scenario 4. Each color represents one single site and the contour lines are two-dimensional kernel density derived from 4,000 random samples from posterior estimate constrained by eddy covariance net CO_2 and CH_4 data (50%, 75%, and 95% distributions) derived from CARDAMOM posterior states and parameters. Refer to Figure 1 for descriptions of lines and intersections.

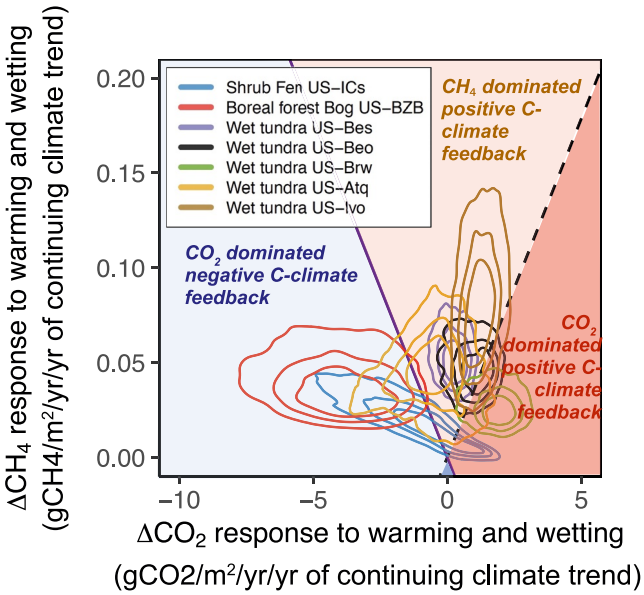

Figure 6. Responses of wetland CO_2 and CH_4 fluxes to continuation of 1970–2016 trends in temperature and precipitation ($+\tau_{temp}$, $+\tau_{prec}$: Scenario 5). See Table 2 for reference to Scenario 5. Each color represents one single site and the contour lines are two-dimensional kernel density derived from 4,000 random samples from posterior estimate constrained by eddy covariance net CO_2 and CH_4 data (50%, 75%, and 95% distributions) derived from CARDAMOM posterior states and parameters. Refer to Figure 1 for descriptions of lines and intersections.

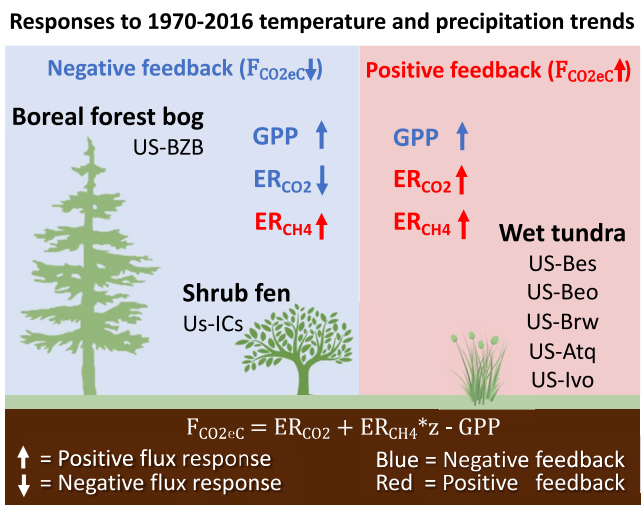

Figure 7. Biogeochemical insight of carbon fluxes responses to continuation of 1970–2016 trends in temperature and precipitation, comparing three different wetland types investigated in this study. GPP is gross primary production. ER_{CO_2} is ecosystem respired CO_2. ER_{CH_4} is ecosystem respired CH_4. Individual site GPP, ER_{CO_2} and ER_{CH_4} flux response values and uncertainties are shown in Figure S14 and Table S2 in Supporting Information S1.

end of century under RCP4.5 and RCP8.5 in CONUS wetlands, which are the same directional changes of CH_4 emission as predicted in our study.

Lawrence et al. (2015) predicted that 10%-drier soil conditions across high-latitude regions will accelerate net CO_2 emissions but strongly suppress growth in CH_4 emissions, resulting in a negative C-climate feedback and a 50% lower F_{CO_2eC}. While our results agree that drier soil (1σ decrease in precipitation) decreases CH_4 emission (with 95% confidence), it affects CO_2 exchange in two directions depending on ecosystem types (Figures 4b and 5b). Specifically, we find that the drier soil conditions result in a negative C-climate feedback across wet tundra sites with a weakening of the gross F_{CO_2eC} by 15%~52% (median of posterior estimations); however, due to the substantial increase in heterotrophic respiration under drier conditions, the boreal forest site exerts a positive C-climate feedback with a 236% increase in the gross F_{CO_2eC} (Figure S14 in Supporting Information S1). Our insights on the control of soil moisture on CH_4 emissions are broadly consistent with Watts et al. (2014), where annual summer CH_4 emission budgets were found to fluctuate by ±4% due to the wet/dry cycles; our 1σ change in annual precipitation swings annual CH_4 emission by ±7% to ±27% (median of posterior estimations) across the seven Alaskan sites.

If the 1970-present warming and wetting trend continues, our results indicate all tundra sites will exhibit a positive gross F_{CO_2eC} response to climate (ΔF_{CO_2eC} = +0.7 to +3.4 gCO_2 eC/m^2/yr per year of continuing climate trend), while the forest (bog) and wet tundra with shrub (fen) sites will have a negative CO_2eC flux response (ΔF_{CO_2eC} = −0.5 to −2.9 gCO_2 eC/m^2/yr per year of continuing climate trend) due to reduced heterotrophic respiration and increased photosynthesis (Figure 6 and Figure S14 in Supporting Information S1). The change of $F_{CO_2eC-CO_2}$ in response to 1970-present climate change is on average 1.5-fold greater than $F_{CO_2eC-CO_2}$ at wet tundra sites but 30% less at the forest and shrub site. Based on 1970-present trends, integrated CH_4 and CO_2 flux sensitivities indicate that high-latitude wetland ecosystems will amplify high-latitude C-climate feedback in wet tundra sites (positive F_{CO_2eC} response) but dampen in boreal forests and lower boundaries of wet tundra sites where shrubs exist (negative CO_2eC response, Figure 7). Both GPP and CH_4 respond positively to the 1970-present climate trends across all seven sites. However, a notable difference between the forest/shrub sites and the tundra sites is their contrasting responses of ER_{CO_2} to climate change. Specifically, in the boreal forest and shrub sites, the ER_{CO_2} response is much larger than the GPP and CH_4 responses (Figure S14 in Supporting Information S1). The negative ER_{CO_2} responses in shrub and forest indicate that the integrated effects of increased precipitation outweigh the effects of rising temperatures, and vice versa for the positive ER_{CO_2} responses in wet tundra ecosystems. We also find that ER_{CO_2} is predominantly driven by heterotrophic respiration flux response: the difference in ER_{CO_2} sensitivities is consistent with differences in underlying heterotrophic sensitivities to precipitation and temperature. We speculate that under current climate conditions, wet tundra respiration increases with increasing soil moisture (moisture response between A and B in Figure S2 in Supporting Information S1), while bog and fen respiration decrease with increasing soil moisture (moisture response between B and C2 in Figure S2 in Supporting Information S1). These contrasting moisture-respiration responses could be due to different soil inundation conditions, subsidence, soil pH, soil redox potential, vegetation types, microbial structures, diurnal or seasonal cycles of fluctuating water table in hummocks and hollows.

To determine if there are substantial differences in climatic sensitivity during the growing/non-growing season, we compared CH_4/CO_2 responses to

climate changes in growing season (June-August) against non-growing seasons (September-May), with similar method we used to quantify averaged annual CH_4/CO_2 response to climate change (see details in supplementary Text S5 in Supporting Information S1). With the continuation of 1970-present climate change trend, US-ICs site (shrub fen) will be a stronger source of CO_2 in the non-growing season and stronger sink of CO_2 in the growing season (Figure S15 in Supporting Information S1). At US-Beo, US-Brw, US-Atq, the directions and magnitudes of CO_2 and CH_4 fluxes in response to climate change are consistent between growing/non-growing seasons. At US-ICs, US-BZB, US-Bes, we find stronger increase of CH_4 in growing seasons than non-growing seasons. We find bigger increase of non-growing season CH_4 than growing season at the US-Ivo site, due to its large shoulder season fluxes (September to December).

The CH_4 GWP metric (Myhre et al., 2013) has been extensively used across investigations to quantify the impact of CH_4 fluxes on the evolution of the Earth System. However, Neubauer and Megonigal (2015) have refined the characterization of the CH_4 radiative forcing impact relative to CO_2, and advocate for a "sustained-flux GWP" (SGWP) metric—to account for the impact of sustained shift in fluxes over time; this amounts to a considerably higher greenhouse gas impact of CH_4 relative to CO_2 (CH_4 SGWP = 45), relative to the GWP assumed in our analysis (CH_4 GWP = 28). To test whether SGWP and GWP metrics lead to consistent or conflicting conclusions on the sign of the inferred C-climate feedback responses in our study, we re-derived the results presented in Figure 7 using a value of $z = 45$ in Equations 15 and 16. The fluxes summarized in Figure 7 (F_{CO_2eC} and component fluxes, namely ER_{CH_4}, ER_{CO_2} and GPP) derived using both SGWP and GWP are presented quantified in Table S2 in Supporting Information S1. While we find that the choice of SGWP and GWP has a substantial impact on both ER_{CH_4} and the overall F_{CO_2eC} fluxes, we find that the sign of the F_{CO_2eC} sensitivity to climate remains unchanged, and therefore our conclusions are not dependent on which CH_4 GWP metric is assumed. We use 100-yr scale GWP value throughout the main text and figures to be consistent with recent wetland CH_4 investigations (Jackson et al., 2020; Lawrence et al., 2015; Peltola et al., 2019; Saunois et al., 2016, 2020; Tian et al., 2016; Webster et al., 2018).

3.4. Future Directions

Overall, our results indicate that accurately resolving both (a) mean CH_4 and CO_2 flux rates across both tundra and boreal ecosystems and (b) their associated climate sensitivity will be critical for determining the sign and magnitude of the northern high latitude ecosystem C-climate feedbacks in the coming decades. Our data-model fusion approach demonstrates joint observational constraints on CO_2 and CH_4, which is the key to understanding ecosystem C cycle responses to the climate in the coming decades. Future studies could use this approach to jointly constrain CO_2 and CH_4 fluxes at a larger number of EC sites with longer records of observations. We emphasize the importance of adding long-term ground and spaceborne observations with better spatial coverage in northern high latitude to constrain terrestrial-atmosphere C balance and the C-climate feedback. While DALEC-JCR does broadly capture the seasonal and IAV of both CH_4 and CO_2 fluxes at all sites, the model does not explicitly represent soil energy dynamics, permafrost thaw, snow cover, snowmelt infiltration, soil consumption of CH_4, soil texture, soil pH, and soil redox potential, which are potentially key for accurately resolving C-H_2O cycle sensitivities to climate. We anticipate that the addition of these processes, along with integrating higher temporal/spatial resolution observations will improve modeled seasonal/inter-annual variations of combined CO_2-CH_4 fluxes and their climate sensitivity.

We infer CH_4 and CO_2 flux sensitivities to climate from the contemporary meteorological forcing and flux and state observations. This derivation assumes linear responses of carbon cycling to climate (Equations 14–16). While the linear sensitivities presented here provide a first-order estimate of flux sensitivity to contemporary climate variability, larger and/or sustained climate perturbations can potentially induce non-linear responses such as (a) non-linear functional responses to climate, for example, heterotrophic temperature and moisture sensitivities or vegetation functional responses (Norton et al., 2023), (b) cumulative legacy effects, and their propagation across the terrestrial carbon cycle states (e.g., productivity increases and subsequently lagged growth of soil organic C states), and (c) long-term processes unrepresented in the model-data integration analysis, for example, shrub expansion, permafrost thaw or nutrient cycling, and/or (d) a shift of ecosystem states beyond a climate threshold or tipping point (Au et al., 2023; Luo et al., 2011). Characterizing the longer-term sensitivities of cumulative CH_4 and CO_2 fluxes to sustained climate change is therefore a key step toward establishing whether (a) contemporary linear responses are the predominant contribution to CH_4 and CO_2 fluxes to climate sensitivity,

or (ii) lagged and/or non-linear process responses to climate change will amount to prominent climate sensitivity terms. Extending the FLUXNET CO_2 and CH_4 data record—along with augmentations in the processes represented in CARDAMOM framework—are key steps toward resolving the integrated CH_4 and CO_2 flux responses to climate change on decadal to centennial timescales.

We highlight that machine learning methods have been used to upscale site-level CO_2/CH_4 emission to regional/global budgets (Peltola et al., 2019; Tramontana et al., 2016); in this context, our MDF approach can potentially be used to investigate the possibility of propagating parameter knowledge from one site to another, supervised by Bayesian probabilities, observations, and physical/biochemical laws from process-based models; this approach could be key to constrain regional/global CH_4 and CO_2 fluxes—and their associated climate sensitivities. We also note that further investigations on the seasonal sensitivities of CO_2-CH_4 fluxes are also needed, given that climate changes may be unique to each season, and that the mechanisms affecting growing/non-growing season fluxes may differ (Natali et al., 2015; Treat et al., 2018a, 2018b; Watts et al., 2014; Zona et al., 2016).

Finally, we highlight that a growing number of satellite greenhouse gas observations can help constrain regional/global CO_2-CH_4 budget and climate sensitivity estimations using our approach, such as wetland CH_4 emissions from inversions of GOSAT data (Ma et al., 2022a; Lu et al., 2021; J. D. Maasakkers et al., 2019; J. Maasakkers et al., 2020; Turner et al., 2015; Y. Zhang et al., 2021) and the GOSAT-derived net biosphere C exchange (NBE) data set (CMS-Flux; Liu et al., 2014, 2018). Furthermore, integration of top-down greenhouse gas flux estimates into land biosphere data-model fusion analyses (e.g., Bloom et al., 2020a, 2020b; Quetin et al., 2020; Yin et al., 2020) can be potentially extend the quantification of CH_4 and CO_2 flux climate sensitivities to regional or global scales.

4. Summary and Conclusions

We find that the CH_4 (in CO_2 equivalent GWP) response to 1970-present climate change is 50% greater than CO_2 at tundra sites but 30% less at the boreal site. Contemporary CH_4 and CO_2 flux sensitivities indicate that high-latitude wetland ecosystems will amplify C-climate feedbacks in tundra but dampen them in boreal forests if the 1970-present climate change trend continues. Precipitation dominates CH_4 sensitivities to climate through changes in the soil moisture. The CO_2 sensitivities are predominantly temperature driven at the tundra sites but are dominated by precipitation (through Rh suppression) at the boreal site.

Our results agree with previous studies that although the amount of CH_4 emissions is about one magnitude smaller than CO_2 on a molar basis, their responses to climate change play an important role in C-climate feedback (X. Zhu et al., 2013; Zhuang et al., 2007). Over the permafrost region, Lawrence et al. (2015) predicted that 10%-drier soil conditions will accelerate net CO_2 emissions but strongly suppress growth in CH_4 emissions, resulting in a negative C-climate feedback and a 50% lower GWP. We find distinct responses of CO_2 emissions to soil moisture changes between wet tundra and forest bog sites, which requires further investigation across individual ecosystem types. Our results highlight the relative importance of both CO_2 and CH_4 biogeochemical sensitivities to climate, which ultimately need to be jointly quantified to accurately resolve the sign and magnitude of high-latitude ecosystem C-climate feedback in the coming decades.

Conflict of Interest

The authors declare no conflicts of interest relevant to this study.

Data Availability Statement

Eddy covariance observation data are available at https://ameriflux.lbl.gov/. Model results are available in a public repository (Ma et al., 2021a, 2021b) (https://doi.org/10.5281/zenodo.6339769). Figures were made with R version 4.2.0 (R Core Team, 2021) (https://www.R-project.org/). Model driver files are derived from the European Centre for Medium-Range Weather Forecasts (ECMWF, 2011) Reanalysis Interim (Berrisford et al., 2011) (https://www.ecmwf.int/en/forecasts/datasets/reanalysis-datasets/era-interim) and are available at https://github.com/CARDAMOM-framework/CARDAMOM_v2.2".

Acknowledgments
Part of this research was carried out at the Jet Propulsion Laboratory, California Institute of Technology, under a contract with the National Aeronautics and Space Administration. Part of the funding for this study was provided through a NASA Terrestrial Ecology Grant NNH21ZDA001N-TE, and NASA Carbon Monitoring System Grants NNH16ZDA001N-CMS and NNH20ZDA001N-CMS. Funding for J.D.W was provided by NASA Terrestrial Ecology Grant 80NSSC22K1245, NNH17ZDA001N and the Gordon and Betty Moore Foundation. Funding for ESE was provided by NSF Grants DEB-1636476, AON 856864, 1304271, 0632264, and 1107892, and the US Geological Survey. Funding for D.Z. was provided by the Office of Polar Programs of the National Science Foundation (NSF) (award numbers 2149988 and 1932900) with additional support by the NASA ABoVE (80NSSC21K1350) Program.

References

Au, J., Bloom, A. A., Parazoo, N. C., Deans, R. M., Wong, C. Y. S., Houlton, B. Z., & Magney, T. S. (2023). Forest productivity recovery or collapse? Model-Data integration insights on drought-induced tipping points. *Global Change Biology*, *29*(19), 1–14. https://doi.org/10.1111/gcb.16867

Aubinet, M., Vesala, T., & Papale, D. (2012). *Eddy covariance: A practical guide to measurement and data analysis*. Springer Science & Business Media.

Beer, C., Ciais, P., Reichstein, M., Baldocchi, D., Law, B. E., Papale, D., et al. (2009). Temporal and among-site variability of inherent water use efficiency at the ecosystem level. *Global Biogeochemical Cycles*, *23*(2), GB2018. https://doi.org/10.1029/2008gb003233

Berrisford, P., Dee, D. P., Poli, P., Brugge, R., Fielding, M., Fuentes, M., et al. (2011). *The ERA-interim archive version 2.0 (ERA report). ERA report series*. ECMWF. Retrieved from https://www.ecmwf.int/node/8174

Bhanja, S. N., & Wang, J. (2020). Estimating influences of environmental drivers on soil heterotrophic respiration in the Athabasca River Basin, Canada. *Environmental Pollution*, *257*, 113630. https://doi.org/10.1016/j.envpol.2019.113630

Bloom, A. A., Bowman, K., Liu, J., Konings, A. G., Worden, J. R., Parazoo, N. C., et al. (2020a). Lagged effects dominate the inter-annual variability of the 2010–2015 tropical carbon balance. *Biogeosciences Discussions*, *2020*(January), 1–49. https://doi.org/10.5194/bg-2019-459

Bloom, A. A., Bowman, K. W., Liu, J., Konings, A. G., Worden, J. R., Parazoo, N. C., et al. (2020b). Lagged effects regulate the inter-annual variability of the tropical carbon balance, 6393–6422.

Bloom, A. A., Bowman, W. K., Lee, M., Turner, J. A., Schroeder, R., Worden, R. J., et al. (2017). A global wetland methane emissions and uncertainty dataset for atmospheric chemical transport models (WetCHARTs version 1.0). *Geoscientific Model Development*, *10*(6), 2141–2156. https://doi.org/10.5194/gmd-10-2141-2017

Bloom, A. A., Exbrayat, J. F., Van Der Velde, I. R., Feng, L., & Williams, M. (2016). The decadal state of the terrestrial carbon cycle: Global retrievals of terrestrial carbon allocation, pools, and residence times. *Proceedings of the National Academy of Sciences of the United States of America*, *113*(5), 1285–1290. https://doi.org/10.1073/pnas.1515160113

Bloom, A. A., & Williams, M. (2015). Constraining ecosystem carbon dynamics in a data-limited world: Integrating ecological "common sense" in a model–data fusion framework. *Biogeosciences*, *12*(5), 1299–1315. https://doi.org/10.5194/bg-12-1299-2015

Bourbonniere, R. A. (2009). Review of water chemistry research in natural and disturbed peatlands. *Canadian Water Resources Journal*, *34*(4), 393–414. https://doi.org/10.4296/cwrj3404393

Box, J. E., Colgan, W. T., Christensen, T. R., Schmidt, N. M., Lund, M., Parmentier, F. J. W., et al. (2019). Key indicators of arctic climate change: 1971–2017. *Environmental Research Letters*, *14*(4), 045010. https://doi.org/10.1088/1748-9326/aafc1b

Braghiere, R. K., Fisher, J. B., Fisher, R. A., Shi, M., Steidinger, B. S., Sulman, B. N., et al. (2021). Mycorrhizal distributions impact global patterns of carbon and nutrient cycling. *Geophysical Research Letters*, *48*(19), 1–11. https://doi.org/10.1029/2021GL094514

Brewer, P. E., Calderón, F., Vigil, M., & von Fischer, J. C. (2018). Impacts of moisture, soil respiration, and agricultural practices on methanogenesis in upland soils as measured with stable isotope pool dilution. *Soil Biology and Biochemistry*, *127*, 239–251. https://doi.org/10.1016/j.soilbio.2018.09.014

Bridgham, S. D., Cadillo-Quiroz, H., Keller, J. K., & Zhuang, Q. (2013). Methane emissions from wetlands: Biogeochemical, microbial, and modeling perspectives from local to global scales. *Global Change Biology*, *19*(5), 1325–1346. https://doi.org/10.1111/gcb.12131

Bridgham, S. D., Megonigal, J. P., Keller, J. K., Bliss, N. B., & Trettin, C. (2006). The carbon balance of North American wetlands. *Wetlands*, *26*(4), 889–916. https://doi.org/10.1672/0277-5212(2006)26[889:tcbona]2.0.co;2

Clymo, R. S., Kramer, J. R., & Hammerton, D. (1984). Sphagnum-dominated peat bog: A naturally acid ecosystem [and discussion]. *Philosophical Transactions of the Royal Society of London. Series B, Biological Sciences*, *305*(1124), 487–499. Retrieved from http://www.jstor.org/stable/2396100

Cox, P. M. (2001). Description of the "TRIFFID" dynamic global vegetation model. *Hadley Centre. Technical Note*, *24*, 17.

Davidson, S. J., Santos, M. J., Sloan, V. L., Watts, J. D., Phoenix, G. K., Oechel, W. C., & Zona, D. (2016). Mapping Arctic tundra vegetation communities using field spectroscopy and multispectral satellite data in North Alaska, USA. *Remote Sensing*, *8*(12), 978. https://doi.org/10.3390/rs8120978

de Vrese, P., Stacke, T., Kleinen, T., & Brovkin, V. (2021). Diverging responses of high-latitude CO_2 and CH_4 emissions in idealized climate change scenarios. *The Cryosphere*, *15*(2), 1097–1130. https://doi.org/10.5194/tc-15-1097-2021

European Centre for Medium-range Weather Forecast (ECMWF). (2011). The ERA-interim reanalysis dataset, Copernicus climate change service (C3S) [Dataset]. ECMWF. Retrieved from https://www.ecmwf.int/en/forecasts/datasets/archive-datasets/reanalysis-datasets/era-interim

Euskirchen, E. S., Bret-Harte, M. S., Shaver, G. R., Edgar, C. W., & Romanovsky, V. E. (2017). Long-term release of carbon dioxide from arctic tundra ecosystems in Alaska. *Ecosystems*, *20*, 960–974. https://doi.org/10.1007/s10021-016-0085-9

Euskirchen, E. S., Edgar, C. W., Turetsky, M. R., Waldrop, M. P., & Harden, J. W. (2014). Differential response of carbon fluxes to climate in three peatland ecosystems that vary in the presence and stability of permafrost. *Journal of Geophysical Research: Biogeosciences*, *119*(8), 1576–1595. https://doi.org/10.1002/2014JG002683

Exbrayat, J.-F., Pitman, A. J., Abramowitz, G., & Wang, Y.-P. (2013). Sensitivity of net ecosystem exchange and heterotrophic respiration to parameterization uncertainty. *Journal of Geophysical Research: Atmospheres*, *118*(4), 1640–1651. https://doi.org/10.1029/2012JD018122

Famiglietti, C., Smallman, T. L., Levine, P., Flack-Prain, S., Quetin, G., Meyer, V., et al. (2020). Optimal model complexity for terrestrial carbon cycle prediction. *Biogeosciences Discussions*, *11*, 1–42. https://doi.org/10.5194/bg-2020-478

Farquharson, L. M., Romanovsky, V. E., Cable, W. L., Walker, D. A., Kokelj, S. V., & Nicolsky, D. (2019). Climate change drives widespread and rapid thermokarst development in very cold permafrost in the Canadian high arctic. *Geophysical Research Letters*, *46*(12), 6681–6689. https://doi.org/10.1029/2019GL082187

Fiedler, S., Vepraskas, M. J., & Richardson, J. L. (2007). Soil redox potential: Importance, field measurements, and observations. *Advances in Agronomy*, *94*, 1–54.

Friedlingstein, P., Meinshausen, M., Arora, V. K., Jones, C. D., Anav, A., Liddicoat, S. K., & Knutti, R. (2014). Uncertainties in CMIP5 climate projections due to carbon cycle feedbacks. *Journal of Climate*, *27*(2), 511–526. https://doi.org/10.1175/JCLI-D-12-00579.1

Gelman, A., & Rubin, D. B. (1992). Inference from iterative simulation using multiple sequences. *Statistical Science*, *7*(4), 457–472. https://doi.org/10.1214/ss/1177011136

Granberg, G., Grip, H., Löfvenius, M. O., Sundh, I., Svensson, B. H., & Nilsson, M. (1999). A simple model for simulation of water content, soil frost, and soil temperatures in boreal mixed mires. *Water Resources Research*, *35*(12), 3771–3782. https://doi.org/10.1029/1999WR900216

Granberg, G., Sundh, I., Svensson, B. H., & Nilsson, M. (2001). Effects of temperature, and nitrogen and sulfur deposition, on methane emission from a boreal mire. *Ecology*, *82*(7), 1982–1998. https://doi.org/10.2307/2680063

Haario, H., Saksman, E., & Tamminen, J. (2001). An adaptive Metropolis algorithm. *Bernoulli*, *7*(2), 223–242. https://doi.org/10.2307/3318737

Hansen, J., Sato, M., Ruedy, R., Lo, K., Lea, D. W., & Medina-Elizade, M. (2006). Global temperature change. *Proceedings of the National Academy of Sciences of the United States of America*, *103*(39), 14288–14293. https://doi.org/10.1073/pnas.0606291103

Hugelius, G., Tarnocai, C., Broll, G., Canadell, J. G., Kuhry, P., & Swanson, D. K. (2013). The northern circumpolar soil carbon database: Spatially distributed datasets of soil coverage and soil carbon storage in the northern permafrost regions. *Earth System Science Data*, *5*(1), 3–13. https://doi.org/10.5194/essd-5-3-2013

Huntzinger, D. N., Michalak, A. M., Schwalm, C., Ciais, P., King, A. W., Fang, Y., et al. (2017). Uncertainty in the response of terrestrial carbon sink to environmental drivers undermines carbon-climate feedback predictions. *Scientific Reports*, *7*(1), 1–8. https://doi.org/10.1038/s41598-017-03818-2

Huntzinger, D. N., Schaefer, K., Schwalm, C., Fisher, J. B., Hayes, D., Stofferahn, E., et al. (2020). Evaluation of simulated soil carbon dynamics in Arctic-Boreal ecosystems. *Environmental Research Letters*, *15*(2), 025005. https://doi.org/10.1088/1748-9326/ab6784

IPCC. (2013). *Climate change 2013: The physical science basis contribution of working group I to the fifth assessment report of the intergovernmental panel on climate change*. Cambridge University Press.

Jackson, R. B., Saunois, M., Bousquet, P., Canadell, J. G., Poulter, B., Stavert, A. R., et al. (2020). Increasing anthropogenic methane emissions arise equally from agricultural and fossil fuel sources. *Environmental Research Letters*, *15*(7), 071002. https://doi.org/10.1088/1748-9326/ab9ed2

Jeong, S. J., Bloom, A. A., Schimel, D., Sweeney, C., Parazoo, N. C., Medvigy, D., et al. (2018). Accelerating rates of arctic carbon cycling revealed by long-term atmospheric CO_2 measurements. *Science Advances*, *4*(7), 1–7. https://doi.org/10.1126/sciadv.aao1167

Keenan, T. F., Davidson, E. A., Munger, J. W., & Richardson, A. D. (2013). Rate my data: Quantifying the value of ecological data for the development of models of the terrestrial carbon cycle. *Ecological Applications*, *23*(1), 273–286. https://doi.org/10.1890/12-0747.1

Knox, S. H., Jackson, R. B., Poulter, B., McNicol, G., Fluet-Chouinard, E., Zhang, Z., et al. (2019). FluXNET-CH_4 synthesis activity objectives, observations, and future directions. *Bulletin of the American Meteorological Society*, *100*(12), 2607–2632. https://doi.org/10.1175/BAMS-D-18-0268.1

Koven, C. D., Hugelius, G., Lawrence, D. M., & Wieder, W. R. (2017). Higher climatological temperature sensitivity of soil carbon in cold than warm climates. *Nature Climate Change*, *7*(11), 817–822. https://doi.org/10.1038/nclimate3421

Laine, A. M., Mäkiranta, P., Laiho, R., Mehtätalo, L., Penttilä, T., Korrensalo, A., et al. (2019). Warming impacts on boreal fen CO_2 exchange under wet and dry conditions. *Global Change Biology*, *25*(6), 1995–2008. https://doi.org/10.1111/gcb.14617

Lawrence, D. M., Koven, C. D., Swenson, S. C., Riley, W. J., & Slater, A. G. (2015). Permafrost thaw and resulting soil moisture changes regulate projected high-latitude CO_2 and CH_4 emissions. *Environmental Research Letters*, *10*(9), 094011. https://doi.org/10.1088/1748-9326/10/9/094011

Lipson, D. A., Zona, D., Raab, T. K., Bozzolo, F., Mauritz, M., & Oechel, W. C. (2012). Water table height and microtopography control Biogeochemical cycling in an Arctic coastal tundra Ecosystem. *Biogeosciences*, *9*(1), 577–591. https://doi.org/10.5194/bg-9-577-2012

Liu, J., Bowman, K., Parazoo, N. C., Bloom, A. A., Wunch, D., Jiang, Z., et al. (2018). Detecting drought impact on terrestrial biosphere carbon fluxes over contiguous US with satellite observations. *Environmental Research Letters*, *13*(9), 095003. https://doi.org/10.1088/1748-9326/aad5ef

Liu, J., Bowman, K. W., Lee, M., Henze, D. K., Bousserez, N., Brix, H., et al. (2014). Carbon monitoring system flux estimation and attribution: Impact of ACOS-GOSAT XCO_2 sampling on the inference of terrestrial biospheric sources and sinks. *Tellus Series B Chemical and Physical Meteorology*, *66*(1), 22486. https://doi.org/10.3402/tellusb.v66.22486

Lu, X., Jacob, D. J., Zhang, Y., Maasakkers, J. D., Sulprizio, M. P., Shen, L., et al. (2021). Global methane budget and trend, 2010–2017: Complementarity of inverse analyses using in situ (GLOBALVIEWplus CH_4 ObsPack) and satellite (GOSAT) observations. *Atmospheric Chemistry and Physics*, *21*(6), 4637–4657. https://doi.org/10.5194/acp-21-4637-2021

Luo, Y., Ogle, K., Tucker, C., Fei, S., Gao, C., LaDeau, S., et al. (2011). Ecological forecasting and data assimilation in a data-rich era. *Ecological Applications*, *21*(5), 1429–1442. https://doi.org/10.1890/09-1275.1

Luo, Y., Shi, Z., Lu, X., Xia, J., Liang, J., Jiang, J., et al. (2017). Transient dynamics of terrestrial carbon storage: Mathematical foundation and its applications. *Biogeosciences*, *14*(1), 145–161. https://doi.org/10.5194/bg-14-145-2017

Ma, S., Bloom, A. A., Quetin, G., Watts, J., Zona, D., Euskirchen, E., et al. (2021a). Resolving the carbon-climate feedback potential of high latitude wetland CO_2 and CH_4 exchanges [Dataset]. Zenodo. https://doi.org/10.5281/zenodo.6339769

Ma, S., Jiang, J., Huang, Y., Shi, Z., Wilson, R. M., Ricciuto, D., et al. (2017). Data-constrained projections of methane fluxes in a northern Minnesota peatland in response to elevated CO_2 and warming. *Journal of Geophysical Research: Biogeosciences*, *122*(11), 2841–2861. https://doi.org/10.1002/2017JG003932

Ma, S., Jiang, L., Wilson, R. M., Chanton, J., Niu, S., Iversen, C. M., et al. (2023). Thermal acclimation of plant photosynthesis and autotrophic respiration in a northern peatland. *Environmental Research: Climate*, *2*(2), 025003. https://doi.org/10.1088/2752-5295/acc67e

Ma, S., Jiang, L., Wilson, R. M., Chanton, J. P., Bridgham, S., Niu, S., et al. (2022). Evaluating alternative ebullition models for predicting peatland methane emission and its pathways via data–model fusion. *Biogeosciences*, *19*(8), 2245–2262. https://doi.org/10.5194/bg-19-2245-2022

Ma, S., Worden, J. R., Bloom, A. A., Zhang, Y., Poulter, B., Cusworth, D. H., et al. (2021b). Satellite constraints on the latitudinal distribution and temperature sensitivity of wetland methane emissions. *AGU Advances*, *2*(3), 1–12. https://doi.org/10.1029/2021av000408

Maasakkers, J. D., Jacob, D., Sulprizio, M., Scarpelli, T., Nesser, H., Sheng, J., et al. (2020). 2010–2015 north American methane emissions, sectoral contributions, and trends: A high-resolution inversion of GOSAT satellite observations of atmospheric methane. *Atmospheric Chemistry and Physics Discussions*, *2*(September), 1–28. https://doi.org/10.5194/acp-2020-915

Maasakkers, J. D., Jacob, D. J., Sulprizio, M. P., Scarpelli, T. R., Nesser, H., Sheng, J. X., et al. (2019). Global distribution of methane emissions, emission trends, and OH concentrations and trends inferred from an inversion of GOSAT satellite data for 2010–2015. *Atmospheric Chemistry and Physics*, *19*(11), 7859–7881. https://doi.org/10.5194/acp-19-7859-2019

Melton, J. R., Wania, R., Hodson, E. L., Poulter, B., Ringeval, B., Spahni, R., et al. (2013). Present state of global wetland extent and wetland methane modelling: Conclusions from a model inter-comparison project (WETCHIMP). *Biogeosciences*, *10*(2), 753–788. https://doi.org/10.5194/bg-10-753-2013

Moyano, F. E., Vasilyeva, N., Bouckaert, L., Cook, F., Craine, J., Curiel Yuste, J., et al. (2012). The moisture response of soil heterotrophic respiration: Interaction with soil properties. *Biogeosciences*, *9*(3), 1173–1182. https://doi.org/10.5194/bg-9-1173-2012

Myhre, G., Shindell, D., Bréon, F.-M., Collins, W., Fuglestvedt, J., Huang, J., et al. (2013). Anthropogenic and natural radiative forcing. In T. F. Stocker, D. Qin, G.-K. Plattner, M. Tignor, S. K. Allen, J. Boschung, et al. (Eds.), *Climate change 2013: The physical science basis. Contribution of working group I to the fifth assessment report of the inter-governmental panel on climate change*. Cambridge University Press.

Natali, S. M., Schuur, E. A. G., Mauritz, M., Schade, J. D., Celis, G., Crummer, K. G., et al. (2015). Permafrost thaw and soil moisture driving CO_2 and CH_4 release from upland tundra. *Journal of Geophysical Research: Biogeosciences*, *120*(3), 525–537. https://doi.org/10.1002/2014JG002872

Neubauer, S. C., & Megonigal, J. P. (2015). Moving beyond global warming potentials to quantify the climatic role of ecosystems. *Ecosystems*, *18*(6), 1000–1013. https://doi.org/10.1007/s10021-015-9879-4

Norton, A. J., Bloom, A. A., Parazoo, N. C., Levine, P. A., Ma, S., Braghiere, R. K., & Smallman, T. L. (2023). Improved process representation of leaf phenology significantly shifts climate sensitivity of ecosystem carbon balance. *Biogeosciences*, *20*(12), 2455–2484. https://doi.org/10.5194/bg-20-2455-2023

Olefeldt, D., Goswami, S., Grosse, G., Hayes, D., Hugelius, G., Kuhry, P., et al. (2016). Circumpolar distribution and carbon storage of thermokarst landscapes. *Nature Communications*, *7*, 1–11. https://doi.org/10.1038/ncomms13043

Peltola, O., Vesala, T., Gao, Y., Räty, O., Alekseychik, P., Aurela, M., et al. (2019). Monthly gridded data product of northern wetland methane emissions based on upscaling eddy covariance observations. *Earth System Science Data Discussions*, *11*, 1–50. https://doi.org/10.5194/essd-2019-28

Piao, S., Ciais, P., Friedlingstein, P., Peylin, P., Reichstein, M., Luyssaert, S., et al. (2008). Net carbon dioxide losses of northern ecosystems in response to autumn warming. *Nature*, *451*(7174), 49–52. https://doi.org/10.1038/nature06444

Porter, G. S., Bajita-Locke, J. B., Hue, N. V., & Strand, D. (2004). Manganese solubility and phytotoxicity affected by soil moisture, oxygen levels, and green manure additions. *Communications in Soil Science and Plant Analysis*, *35*(1–2), 99–116. https://doi.org/10.1081/CSS-120027637

Quan, Q., Tian, D., Luo, Y., Zhang, F., Crowther, T. W., Zhu, K., et al. (2019). Water scaling of ecosystem carbon cycle feedback to climate warming. *Science Advances*, *5*(8), 1–8. https://doi.org/10.1126/sciadv.aav1131

Quetin, G. R., Bloom, A. A., Bowman, K. W., & Konings, A. G. (2020). Carbon flux variability from a relatively simple ecosystem model with assimilated data is consistent with terrestrial biosphere model estimates. *Journal of Advances in Modeling Earth Systems*, *12*(3). https://doi.org/10.1029/2019MS001889

R Core Team. (2021). R: A language and environment for statistical computing [Software]. R Foundation for Statistical Computing, Vienna, Austria. Retrieved from https://www.R-project.org

Reich, P. B., Sendall, K. M., Stefanski, A., Rich, R. L., Hobbie, S. E., & Montgomery, R. A. (2018). Effects of climate warming on photosynthesis in boreal tree species depend on soil moisture. *Nature*, *562*(7726), 263–267. https://doi.org/10.1038/s41586-018-0582-4

Riley, W. J., Subin, Z. M., Lawrence, D. M., Swenson, S. C., Torn, M. S., Meng, L., et al. (2011). Barriers to predicting changes in global terrestrial methane fluxes: Analyses using CLM4Me, a methane biogeochemistry model integrated in CESM. *Biogeosciences*, *8*(7), 1925–1953. https://doi.org/10.5194/bg-8-1925-2011

Rodenhizer, H., Ledman, J., Mauritz, M., Natali, S. M., Pegoraro, E., Plaza, C., et al. (2020). Carbon thaw rate doubles when accounting for subsidence in a permafrost warming experiment. *Journal of Geophysical Research: Biogeosciences*, *125*(6), 1–16. https://doi.org/10.1029/2019JG005528

Saunois, M., Bousquet, P., Poulter, B., Peregon, A., Ciais, P., Canadell, J. G., et al. (2016). The global methane budget 2000–2012. *Earth System Science Data*, *8*(2), 697–751. https://doi.org/10.5194/essd-8-697-2016

Saunois, M., Stavert, R. A., Poulter, B., Bousquet, P., Canadell, G. J., Jackson, B. R., et al. (2020). The global methane budget 2000–2017. *Earth System Science Data*, *12*(3), 1561–1623. https://doi.org/10.5194/essd-12-1561-2020

Schädel, C., Schuur, E. A. G., Bracho, R., Elberling, B., Knoblauch, C., Lee, H., et al. (2014). Circumpolar assessment of permafrost C quality and its vulnerability over time using long-term incubation data. *Global Change Biology*, *20*(2), 641–652. https://doi.org/10.1111/gcb.12417

Schuur, E. A. G., McGuire, A. D., Schädel, C., Grosse, G., Harden, J. W., Hayes, D. J., et al. (2015). Climate change and the permafrost carbon feedback. *Nature*, *520*(7546), 171–179. https://doi.org/10.1038/nature14338

Shu, S., Jain, A. K., & Kheshgi, H. S. (2020). Investigating wetland and nonwetland soil methane emissions and sinks across the contiguous United States using a land Surface model. *Global Biogeochemical Cycles*, *34*(7), e2019GB006251. https://doi.org/10.1029/2019GB006251

Sitch, S., Smith, B., Prentice, I. C., Arneth, A., Bondeau, A., Cramer, W., et al. (2003). Evaluation of ecosystem dynamics, plant geography and terrestrial carbon cycling in the LPJ dynamic global vegetation model. *Global Change Biology*, *9*(2), 161–185. https://doi.org/10.1046/j.1365-2486.2003.00569.x

Smallman, T. L., Exbrayat, J.-F., Mencuccini, M., Bloom, A. A., & Williams, M. (2017). Assimilation of repeated woody biomass observations constrains decadal ecosystem carbon cycle uncertainty in aggrading forests. *Journal of Geophysical Research: Biogeosciences*, *122*(3), 528–545. https://doi.org/10.1002/2016JG003520

Stettz, S., Parazoo, N., Bloom, A. A., Blanken, P., Bowling, D., Burns, S., et al. (2021). Resolving temperature limitation on spring productivity in an evergreen conifer forest using a model-data fusion framework. *Biogeosciences Discussions*, *2021*, 1–24. https://doi.org/10.5194/bg-2021-152

Tian, H., Lu, C., Ciais, P., Michalak, A. M., Canadell, J. G., Saikawa, E., et al. (2016). The terrestrial biosphere as a net source of greenhouse gases to the atmosphere. *Nature*, *531*(7593), 225–228. https://doi.org/10.1038/nature16946

Todd-Brown, K. E. O., Randerson, J. T., Post, W. M., Hoffman, F. M., Tarnocai, C., Schuur, E. A. G., & Allison, S. D. (2013). Causes of variation in soil carbon simulations from CMIP5 Earth system models and comparison with observations. *Biogeosciences*, *10*(3), 1717–1736. https://doi.org/10.5194/bg-10-1717-2013

Tramontana, G., Jung, M., Schwalm, C. R., Ichii, K., Camps-Valls, G., Ráduly, B., et al. (2016). Predicting carbon dioxide and energy fluxes across global FLUXNET sites with regression algorithms. *Biogeosciences*, *13*(14), 4291–4313. https://doi.org/10.5194/bg-13-4291-2016

Treat, C. C., Bloom, A. A., & Marushchak, M. E. (2018a). Nongrowing season methane emissions–a significant component of annual emissions across northern ecosystems. *Global Change Biology*, *24*(8), 3331–3343. https://doi.org/10.1111/gcb.14137

Treat, C. C., Marushchak, M. E., Voigt, C., Zhang, Y., Tan, Z., Zhuang, Q., et al. (2018b). Tundra landscape heterogeneity, not interannual variability, controls the decadal regional carbon balance in the Western Russian Arctic. *Global Change Biology*, *24*(11), 5188–5204. https://doi.org/10.1111/gcb.14421

Turetsky, M. R., Treat, C. C., Waldrop, M. P., Waddington, J. M., Harden, J. W., & McGuire, A. D. (2008). Short-term response of methane fluxes and methanogen activity to water table and soil warming manipulations in an Alaskan peatland. *Journal of Geophysical Research*, *113*, G00A10. https://doi.org/10.1029/2007JG000496

Turetsky, M. R., Weider, R. K., Vitt, D. H., Evans, R. J., & Scott, K. D. (2007). The disappearance of relict permafrost in boreal North America: Effects on peatland carbon storage and fluxes. *Global Change Biology*, *13*(9), 1922–1934. https://doi.org/10.1111/j.1365-2486.2007.01381.x

Turner, A. J., Jacob, D. J., Wecht, K. J., Maasakkers, J. D., Lundgren, E., Andrews, A. E., et al. (2015). Estimating global and North American methane emissions with high spatial resolution using GOSAT satellite data. *Atmospheric Chemistry and Physics*, *15*(12), 7049–7069. https://doi.org/10.5194/acp-15-7049-2015

Updegraff, K., Bridgham, S. D., Pastor, J., Weishampel, P., & Harth, C. (2001). Response of CO_2 and CH_4 emissions from peatlands to warming and water table manipulation. *Ecological Applications*, *11*(2), 311–326. https://doi.org/10.1890/1051-0761(2001)011%5B0311:ROCACE%5D2.0

Verville, J. H., Hobbie, S. E., Chapin, F. S., & Hooper, D. U. (1998). Response of tundra CH_4 and CO_2 flux to manipulation of temperature and vegetation. *Biogeochemistry*, *41*(3), 215–235. https://doi.org/10.1023/a:1005984701775

Vuichard, N., & Papale, D. (2015). Filling the gaps in meteorological continuous data measured at FLUXNET sites with ERA-Interim reanalysis. *Earth System Science Data*, *7*(2), 157–171. https://doi.org/10.5194/essd-7-157-2015

Wang, Y., Yuan, F., Yuan, F., Gu, B., Hahn, M. S., Torn, M. S., et al. (2019). Mechanistic modeling of microtopographic impacts on CO_2 and CH_4 fluxes in an Alaskan tundra ecosystem using the CLM-microbe model. *Journal of Advances in Modeling Earth Systems*, *11*(12), 4228–4304. https://doi.org/10.1029/2019ms001771

Wania, R., Ross, I., & Prentice, I. C. (2010). Implementation and evaluation of a new methane model within a dynamic global vegetation model: LPJ-WHyMe v1. 3.1. *Geoscientific Model Development*, *3*(2), 565–584. https://doi.org/10.5194/gmd-3-565-2010

Watts, J. D., Kimball, J. S., Bartsch, A., & McDonald, K. C. (2014). Surface water inundation in the boreal-Arctic: Potential impacts on regional methane emissions. *Environmental Research Letters*, *9*(7), 075001. https://doi.org/10.1088/1748-9326/9/7/075001

Webster, K. L., Bhatti, J. S., Thompson, D. K., Nelson, S. A., Shaw, C. H., Bona, K. A., et al. (2018). Spatially-integrated estimates of net ecosystem exchange and methane fluxes from Canadian peatlands. *Carbon Balance and Management*, *13*(1), 16. https://doi.org/10.1186/s13021-018-0105-5

Weng, E., & Luo, Y. (2008). Soil hydrological properties regulate grassland ecosystem responses to multifactor global change: A modeling analysis. *Journal of Geophysical Research*, *113*(G3), G03003. https://doi.org/10.1029/2007JG000539

Whalen, S. C. (2005). Biogeochemistry of methane exchange between natural wetlands and the atmosphere. *Environmental Engineering Science*, *22*(1), 73–94. https://doi.org/10.1089/ees.2005.22.73

Wieder, W. R., Sulman, B. N., Hartman, M. D., Koven, C. D., & Bradford, M. A. (2019). Arctic soil governs whether climate change drives global losses or gains in soil carbon. *Geophysical Research Letters*, *46*(24), 14486–14495. https://doi.org/10.1029/2019GL085543

Williams, M., Schwarz, P. A., Law, B. E., Irvine, J., & Kurpius, M. R. (2005). An improved analysis of forest carbon dynamics using data assimilation. *Global Change Biology*, *11*(1), 89–105. https://doi.org/10.1111/j.1365-2486.2004.00891.x

Xu, X., Yuan, F., Hanson, P. J., Wullschleger, S. D., Thornton, P. E., Riley, W. J., et al. (2016). Review and Synthesis: Four decades of modeling methane cycling within terrestrial ecosystems. *Biogeosciences*, *13*(12), 3735–3755. https://doi.org/10.5194/bg-13-3735-2016

Yang, Y., Bloom, A. A., Ma, S., Levine, P., Norton, A., Parazoo, N., et al. (2021). CARDAMOM-FluxVal version 1.0: A FLUXNET-based validation system for CARDAMOM carbon and water flux estimates. *Geoscientific Model Development Discussions*, *2021*(July), 1–25. https://doi.org/10.5194/gmd-2021-190

Yin, Y., Bloom, A. A., Worden, J., Saatchi, S., Yang, Y., Williams, M., et al. (2020). Fire decline in dry tropical ecosystems enhances decadal land carbon sink. *Nature Communications*, *11*(1), 1–7. https://doi.org/10.1038/s41467-020-15852-2

Yvon-Durocher, G., Allen, A. P., Bastviken, D., Conrad, R., Gudasz, C., St-Pierre, A., et al. (2014). Methane fluxes show consistent temperature dependence across microbial to ecosystem scales. *Nature*, *507*(7493), 488–491. https://doi.org/10.1038/nature13164

Zhang, H., Väliranta, M., Piilo, S., Amesbury, M. J., Aquino-López, M. A., Roland, T. P., et al. (2020). Decreased carbon accumulation feedback driven by climate-induced drying of two southern boreal bogs over recent centuries. *Global Change Biology*, *26*(4), 2435–2448. https://doi.org/10.1111/gcb.15005

Zhang, Y., Jacob, D. J., Lu, X., Maasakkers, D. J., Scarpelli, T. R., Sheng, J. X., et al. (2021). Attribution of the accelerating increase in atmospheric methane during 2010-2018 by inverse analysis of GOSAT observations. *Atmospheric Chemistry and Physics*, *21*(5), 3643–3666. https://doi.org/10.5194/acp-21-3643-2021

Zhu, Q., Liu, J., Peng, C., Chen, H., Fang, X., Jiang, H., et al. (2014). Modelling methane emissions from natural wetlands by development and application of the TRIPLEX-GHG model. *Geoscientific Model Development*, *7*(3), 981–999. https://doi.org/10.5194/gmd-7-981-2014

Zhu, X., Zhuang, Q., Gao, X., Sokolov, A., & Schlosser, C. A. (2013). Pan-Arctic land-atmospheric fluxes of methane and carbon dioxide in response to climate change over the 21st century. *Environmental Research Letters*, *8*(4), 045003. https://doi.org/10.1088/1748-9326/8/4/045003

Zhuang, Q., Melillo, J. M., McGuire, A. D., Kicklighter, D. W., Prinn, R. G., Steudler, P. A., et al. (2007). Net emissions of CH_4 and CO_2 in Alaska: Implications for the region's greenhouse gas budget. *Ecological Applications*, *17*(1), 203–212. https://doi.org/10.1890/1051-0761(2007)017[0203:NEOCAC]2.0.CO;2

Zona, D., Gioli, B., Commane, R., Lindaas, J., Wofsy, S. C., Miller, C. E., et al. (2016). Cold season emissions dominate the Arctic tundra methane budget. *Proceedings of the National Academy of Sciences of the United States of America*, *113*(1), 40–45. https://doi.org/10.1073/pnas.1516017113

Erratum

The supporting information file in the originally published version of this article displayed edits made with tracked changes. The file has been replaced, and this version may be considered the authoritative version of record.